Supporting Information

Investing in Entropy: The Strategy of Cucurbit[*n*]urils to Accelerate the Intramolecular Diels-Alder Cycloaddition Reaction of Tertiary Furfuryl Amines

Karen de la Vega-Hernández,[a] Marcos G. Suero,*[a,b] and Pablo Ballester*[a,b]

[a] *Institute of Chemical Research of Catalonia (ICIQ-CERCA), The Barcelona Institute of Science and Technology (BIST), Avgda. Països Catalans 16, 43007, Tarragona, Spain.*

[b] *ICREA, Passeig Lluís Companys, 23, 08018 Barcelona, Spain.*

Table of Contents

I	**General Information**	**S4**
II	**Synthesis and Characterization Data**	**S5**
III	**Binding Studies**	**S11**
III.1	General Procedure for ^{1}H NMR Titrations	S11
III.2	Binding Studies of FA-1 with CB[7]	S11
III.3	Binding Studies of P-1 with CB[7] and DOSY Results	S13
III.4	Binding Studies of FA-2 with CB[7]	S14
III.5	Binding Studies of P-2 with CB[7] and DOSY Results	S16
III.6	Binding Studies of FA-1 with CB[8]	S17
III.7	Binding Studies of FA-2 with CB[8]	S18
III.8	Isothermal Titration Calorimetry (ITC) Experiments of FA-1 and P-1 with CB[7]	S19
III.9	Competitive Experiment of P-2⊂CB[7] with P-1	S23
III.10	Kinetic Characterization of the Complexes FA-1⊂CB[7] and P-1⊂CB[7]	S24
IV	**Theoretical Kinetic Models Used in the Fits and Simulations of the Reaction Profiles**	**S26**
V	**Kinetic Studies of FA-1 with CB[7]**	**S28**
V.1	General Procedure for Kinetic Experiments	S28
V.2	Kinetic Profiles	S28
V.3	Competitive Displacement of the Bound Product	S30
V.4	Control Experiment	S30
V.5	Kinetics upon Catalytic Amount of CB[7]	S32
V.6	Determination of Activation Parameters under Standard Reaction Conditions	S33
V.7	Derivation of the Rate Law	S37
VI	**Kinetic Studies of FA-2 with CB[7]**	**S39**
VI.1	Kinetic Profiles	S39
VI.2	Competitive Displacement of the Bound Product	S40
VI.3	Control Experiment	S41

VI.4	Kinetics upon Catalytic Amount of CB[7]	S42
VI.5	Determination of Activation Parameters under Standard Reaction Conditions	S45
VII	**Kinetic Studies of FA-1 with CB[8]**	**S48**
VIII	**Kinetic Studies of FA-2 with CB[8]**	**S50**
IX	**Kinetic Data and CB[*n*]-promoted acceleration ($k_{included}/k_{bulk}$) of the IMDA cycloaddition reactions of FA-1 and FA-2**	**S51**
X	**Binding and Kinetic Studies of FA-1 with Cyclodextrins**	**S52**
XI	**Energy-Minimized Structures of the Inclusion Complexes with CB[*n*]s**	**S57**

I. General Information

Reagents and solvents were purchased from commercial sources and used without prior purification: cucurbit[7]uril (**CB[7]**: Sigma-Aldrich, abcr or BLD PHARMATECH GmbH), cucurbit[8]uril (**CB[8]**: Sigma-Aldrich or abcr), *N*-(furan-2-ylmethyl)-*N*-methylprop-2-en-1-amine (**FA-1**: Chemspace), and *N*-(furan-2-ylmethyl)-*N*-methylbut-3-en-1-amine (**FA-2**: Chemspace). Routine ^{1}H NMR and ^{13}C{^{1}H} NMR spectra were recorded on a Bruker Avance 300 (300 MHz for ^{1}H NMR and 75 MHz for ^{13}C NMR) or Bruker Avance 400 (400 MHz for ^{1}H NMR and 100 MHz for ^{13}C NMR). Deuterated solvents used are indicated in the characterization and chemical shifts are given in ppm. Residual solvent peaks were used as reference. Data are reported as follows: chemical shift, multiplicity (s = singlet, d = doublet, t = triplet, m = multiplet), coupling constant (Hz) and integration. COSY, NOESY, ROESY, HSQC and HMBC experiments were recorded to help with the assignment of ^{1}H and ^{13}C signals. High Resolution Mass Spectra (HRMS) were obtained on a Bruker HPLC-ESI-TOF (MicroTOF Focus). ITC experiments were performed using a MicroCal VP-ITC MicroCalorimeter with the VP Viewer 2000 software, MicroCal, version 7.0, Northampton, MA, USA. Milli-Q water was used for the preparation of all non-deuterated aqueous solutions. The kinetic data was analyzed using the initial rates method and/or academic commercial software packages (COPASI 4.25) to determine the rate constants of the reactions under study.

II. Synthesis and Characterization Data

For ease of reference, the full characterization of tertiary furfuryl amines **FA-1** and **FA-2** are included hereafter.

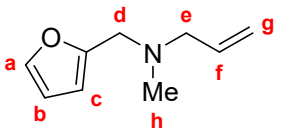

FA-1

***N*-(furan-2-ylmethyl)-*N*-methylprop-2-en-1-amine (FA-1):**

^{1}H NMR (400 MHz, D_2O): δ 7.52 (dd, *J* = 1.9 Hz, *J* = 0.8 Hz, 1H), 6.47 (dd, *J* = 3.2 Hz, *J* = 1.9 Hz, 1H), 6.39 (dd, *J* = 3.2 Hz, *J* = 0.8 Hz, 1H), 5.91 (ddt, *J* = 17.1 Hz, *J* = 10.2 Hz, *J* = 6.8 Hz, 1H), 5.33–5.25 (m, 2H), 3.62 (s, 2H), 3.09 (dt, *J* = 6.8 Hz, *J* = 1.2 Hz, 2H), 2.22 (s, 3H).

^{13}C{^{1}H} NMR (100 MHz, D_2O): δ 151.3, 142.7, 133.9, 119.2, 110.3, 109.5, 58.7, 51.7, 40.5.

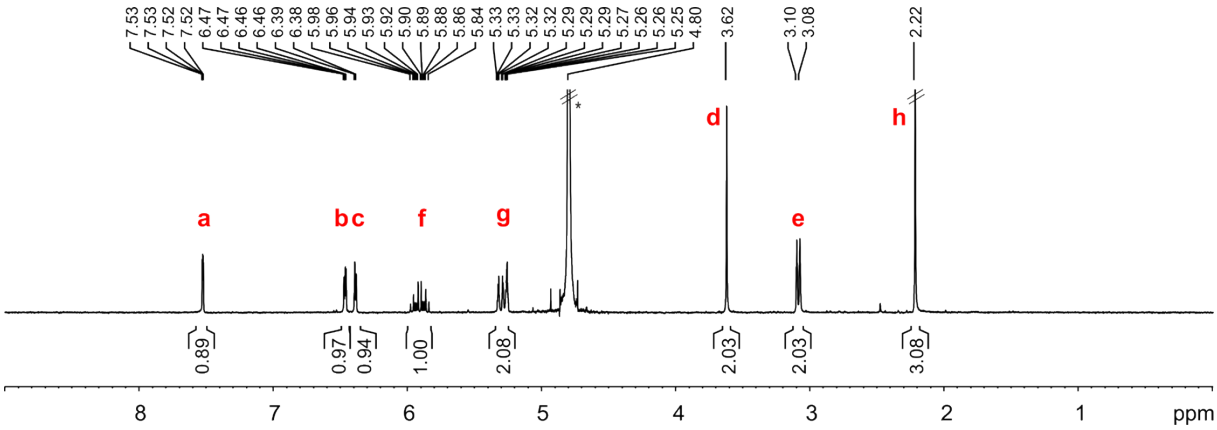

Figure S1. ^{1}H NMR spectrum (400 MHz, D_2O, 298 K) of **FA-1**. *Residual solvent peak.

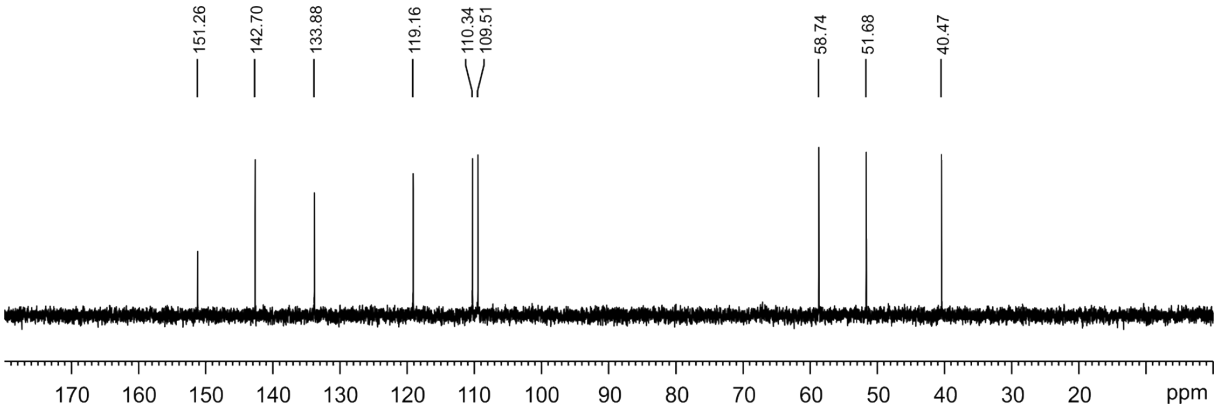

Figure S2. $^{13}C\{^{1}H\}$ NMR spectrum (100 MHz, D_2O, 298 K) of **FA-1**.

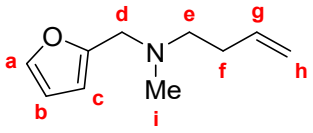

FA-2

***N*-(furan-2-ylmethyl)-*N*-methylbut-3-en-1-amine (FA-2):**

^{1}H NMR (400 MHz, D_2O): δ 7.53 (dd, *J* = 1.9 Hz, *J* = 0.9 Hz, 1H), 6.48–6.46 (m, 1H), 6.41–6.40 (m, 1H), 5.84 (ddt, *J* = 17.1 Hz, *J* = 10.2 Hz, *J* = 6.7 Hz, 1H), 5.18–5.04 (m, 2H), 3.67 (s, 2H), 2.57–2.51 (m, 2H), 2.34–2.26 (m, 2H), 2.27 (s, 3H).

^{13}C{^{1}H} NMR (100 MHz, D_2O): δ 151.1, 142.7, 136.7, 115.8, 110.3, 109.6, 55.0, 52.0, 40.8, 30.4.

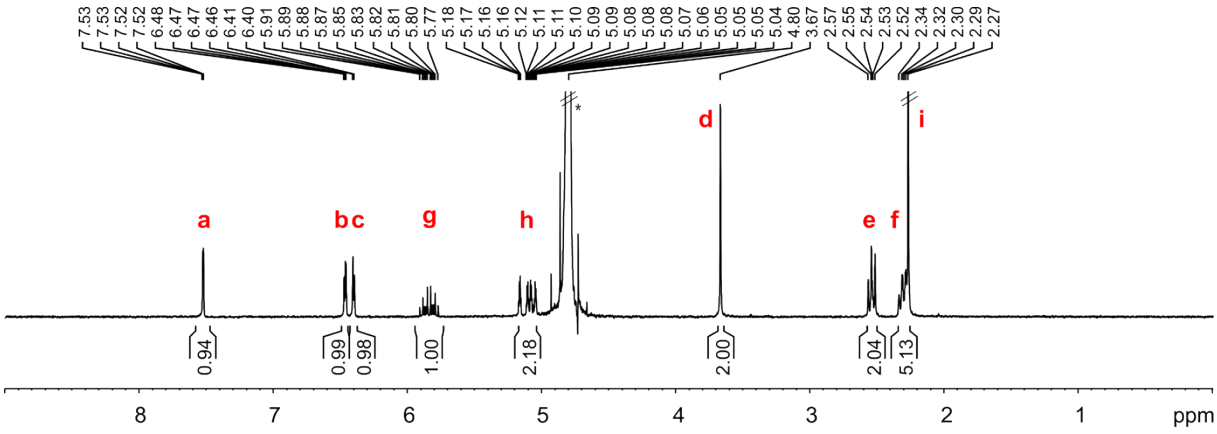

Figure S3. ^{1}H NMR spectrum (400 MHz, D_2O, 298 K) of **FA-2**. *Residual solvent peak.

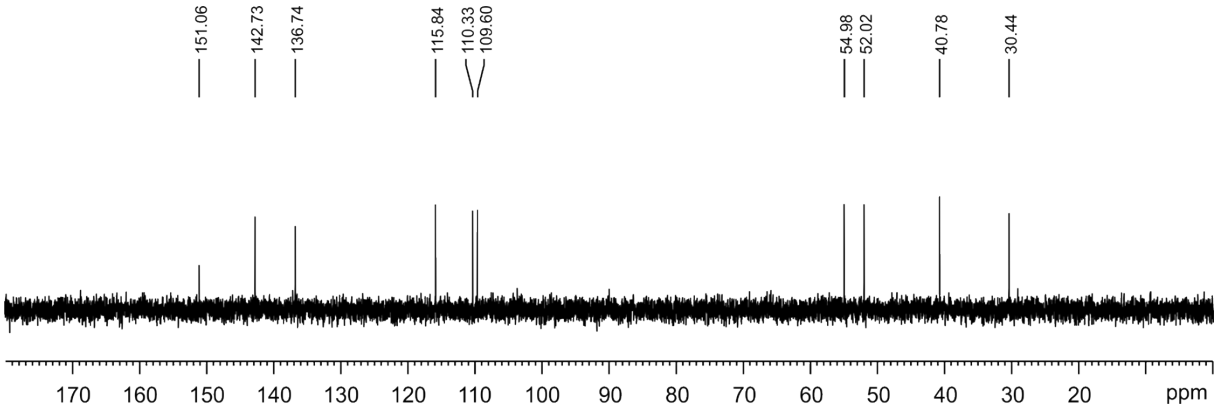

Figure S4. $^{13}C\{^{1}H\}$ NMR spectrum (100 MHz, D_2O, 298 K) of **FA-2**.

For guest uptake studies and full characterization, the Diels-Alder cycloaddition product **P-1** was synthesized as follows: in an NMR tube, tertiary furfuryl amine **FA-1** (5.0 mM solution in D_2O, 600 μL) was placed in an oil bath pre-heated at 343 K. The solution was heated until the reaction reached completion (14 days).

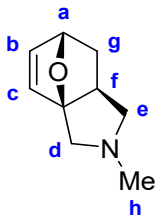

$C_9H_{13}NO$

M = 151.21 g·mol^{-1}

P-1

rac-(3aS,6S,7aS)-2-methyl-1,2,3,6,7,7a-hexahydro-3a,6-epoxyisoindole (P-1):

^{1}H NMR (400 MHz, D_2O): δ 6.54 (d, *J* = 5.9 Hz, 1H), 6.44 (dd, *J* = 5.9 Hz, *J* = 1.8 Hz, 1H), 5.14 (dd, *J* = 4.6 Hz, *J* = 1.8 Hz, 1H), 3.68 (d, *J* = 13.1 Hz, 1H), 3.29 (dd, *J* = 9.8 Hz, *J* = 7.1 Hz, 1H), 2.81 (d, *J* = 13.1 Hz, 1H), 2.50 (s, 3H), 2.33 (t, *J* = 10.2 Hz, 1H), 2.20–2.13 (m, 1H), 1.82–1.77 (m, 1H), 1.49 (dd, *J* = 11.9 Hz, *J* = 7.9 Hz, 1H).

^{13}C{^{1}H} NMR (100 MHz, D_2O): δ 136.3, 134.6, 97.2, 80.6, 59.7, 55.3, 43.3, 41.1, 28.6.

HRMS (ESI): *m*/*z* calculated for $[C_9H_{13}NO+H]^+$ 152.1070; found 152.1074.

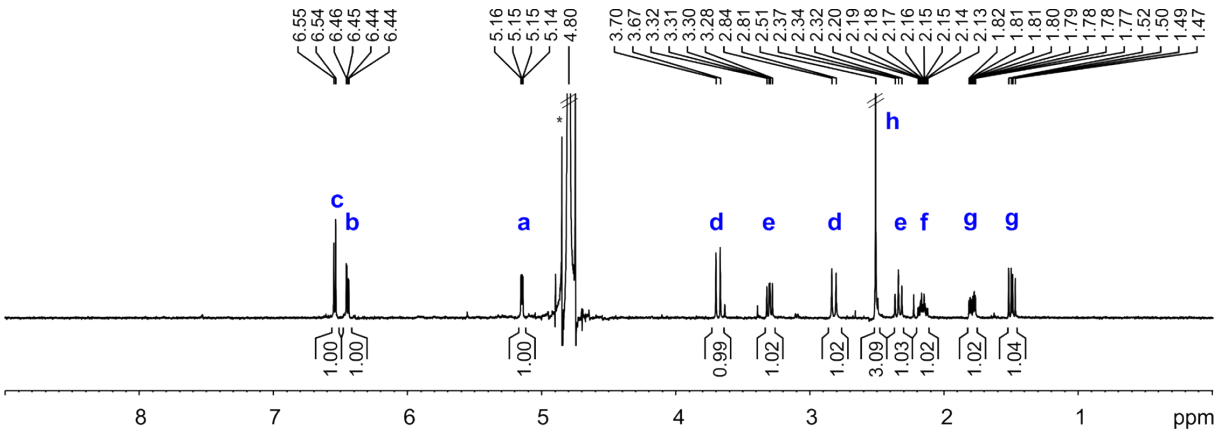

Figure S5. ^{1}H NMR spectrum (400 MHz, D_2O, 298 K) of the Diels-Alder product **P-1**. *Residual solvent peak.

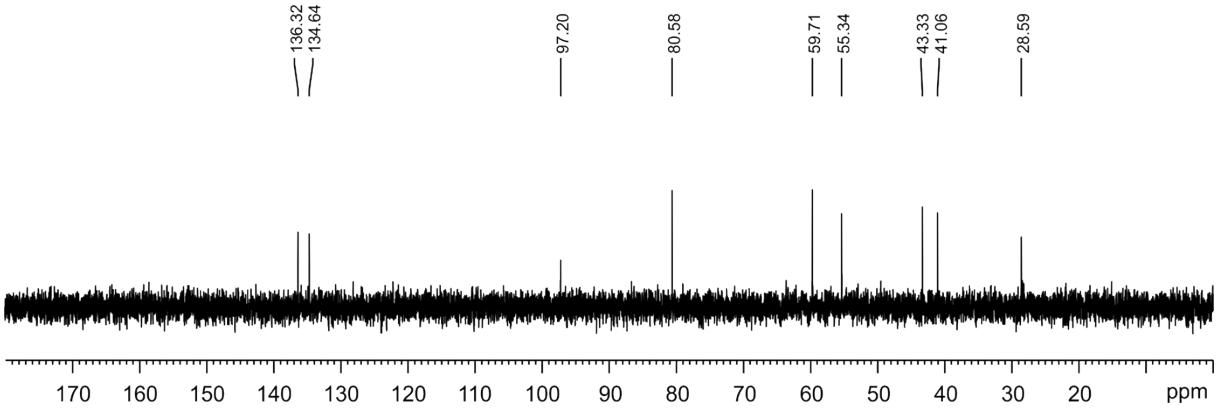

Figure S6. $^{13}C\{^{1}H\}$ NMR spectrum (100 MHz, D_2O, 298 K) of the Diels-Alder product **P-1**.

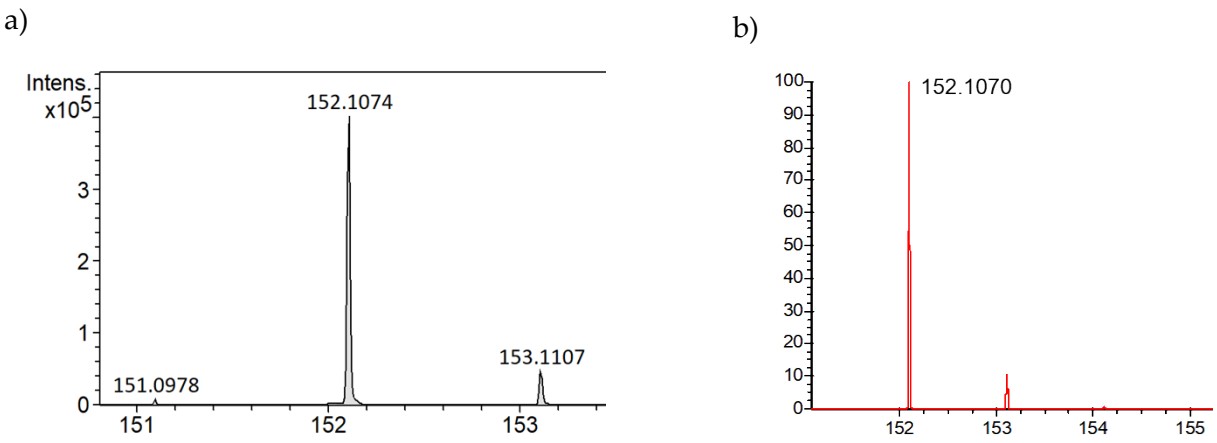

Figure S7. a) Experimental and b) theoretical isotopic distributions for $[M+H]^+$ of **P-1**. The exact mass for the monoisotopic peak in a) and b) is indicated.

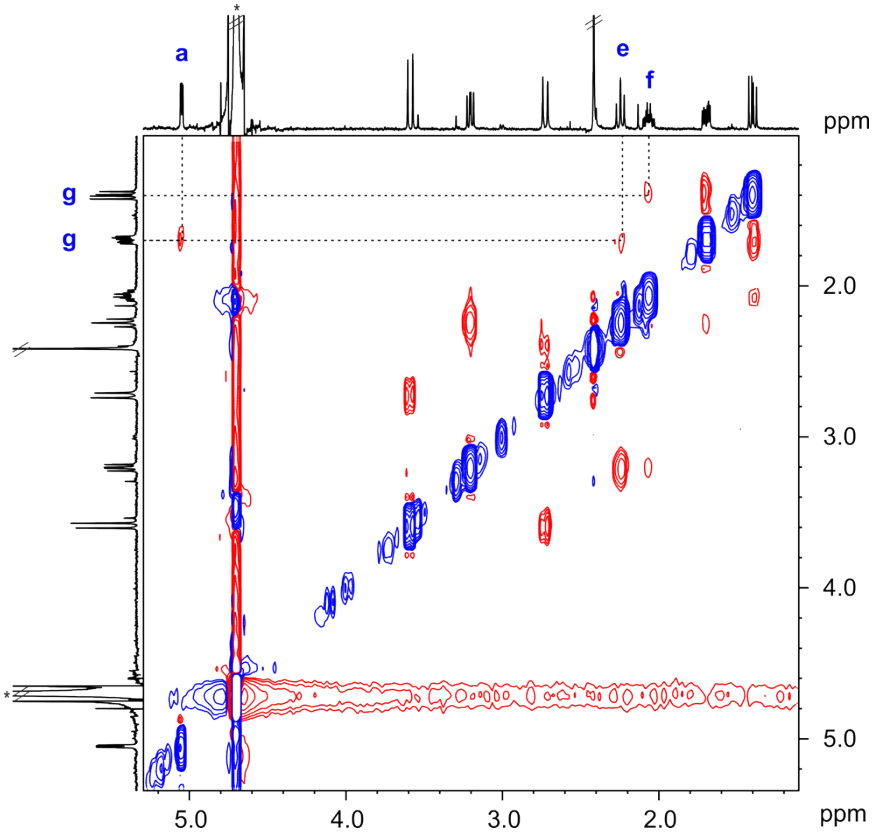

Figure S8. Selected region of the ^{1}H-^{1}H NOESY NMR spectrum (400 MHz, D_2O, 298 K) of the Diels-Alder product **P-1**.

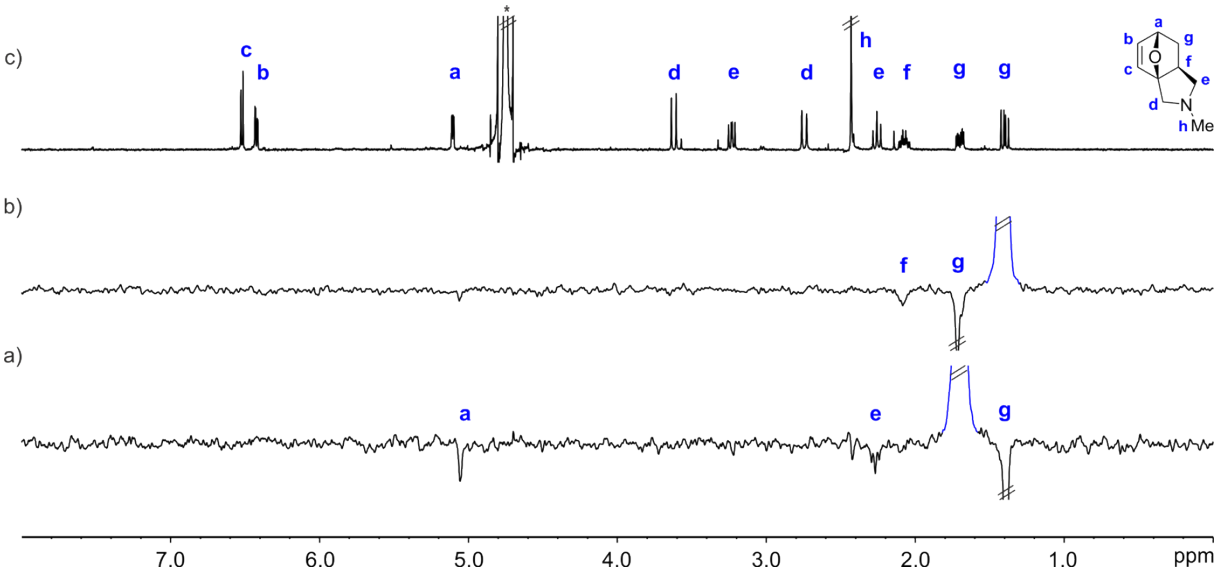

Figure S9. GOESY NMR spectra (400 MHz, D_2O, 298 K) of the Diels-Alder product **P-1**, with selective pulses centered on peaks: a) 1.696 ppm, and b) 1.399 ppm. c) ^{1}H NMR spectrum of **P-1**.

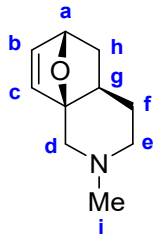

$C_{10}H_{15}NO$

$M = 165.24\ g \cdot mol^{-1}$

P-2

rac-(4aR,6S,8aR)-2-methyl-2,3,4,4a,5,6-hexahydro-1H-6,8a-epoxyisoquinoline (P-2):

Despite our efforts, we were not able to isolate product **P-2** in pure form. The ^{1}H NMR spectrum of compound **P-2** is included beneath as a mixture with **CB[7]** and 2-adamantanone (see also Figure S16).

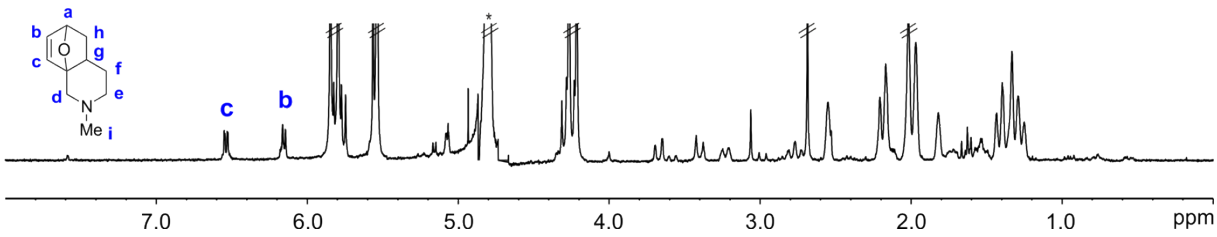

Figure S10. ^{1}H NMR spectrum (400 MHz, D_2O, 298 K) of **P-2** (in a mixture with **CB[7]** and 2-adamantanone (**ADA**)). *Residual solvent peak.

III. Binding Studies

III.1 General Procedure for ^{1}H NMR Titrations

A solution of **CB[7]** (10 mM) was prepared in D_2O. Subsequently, 0.3 mL of the solution of the host were transferred to different NMR tubes. In parallel, three solutions of each guest at different concentrations (5.0 mM, 10 mM, and 20 mM) were also prepared in D_2O. Next, 0.3 mL of each solution of the guest were transferred to three independent NMR tubes already containing the host. In this manner, the total volume in each NMR tube was 0.6 mL, with a final concentration of 5.0 mM (host), and final concentrations of 2.5 mM (0.5 equiv.), 5.0 mM (1.0 equiv.), and 10 mM (2.0 equiv.), respectively, of the guests. The samples were vortexed three times and inserted immediately into the NMR for analysis where ^{1}H NMR spectra (400 MHz) were acquired.

Due to the lower solubility of **CB[8]** in water, a solution of the host (5.0 mM) was prepared in D_2O, along with three solutions of the guests at different concentrations (2.5 mM, 5.0 mM, and 10 mM). Similarly, 0.3 mL of the host plus 0.3 mL of the guest (at different concentrations) were then transferred to independent NMR tubes to achieve a final concentration of 2.5 mM (host), and final concentrations of 1.25 mM (0.5 equiv.), 2.5 mM (1.0 equiv.), and 5.0 mM (2.0 equiv.), respectively, of the guests.

When the binding process showed intermediate/fast exchange dynamics on the ^{1}H NMR chemical shift timescale, the apparent binding constants were determined from the fit of the chemical shift changes observed during the titration to a 1:1 theoretical binding model. We used HypNMR2008 software, Hyperquad, version 4.0.66, Leeds, England, UK, for the fitting procedure.

III.2 Binding Studies of FA-1 with CB[7]

In the initial phase of the titration, the formation of **FA-1⊂CB[7]** complex was demonstrated by the observation of a new set of signals corresponding to the bound guest. Upon the addition of 1.0 equiv. of **FA-1**, only the proton signals of the bound guest were detected. The addition of more than 1.0 equiv. of **FA-1** did not produce additional changes in the signals of the bound

guest but the appearance of the proton signals of the free guest. Taken together, these observations indicated that: (i) **FA-1** and **CB[7]** formed a 1:1 inclusion complex, (ii) the binding process displayed slow exchange dynamics on the ^{1}H NMR chemical-shift timescale, and (iii) the binding constant of the formed complex can be estimated to be larger than 10^4 M^{-1}.

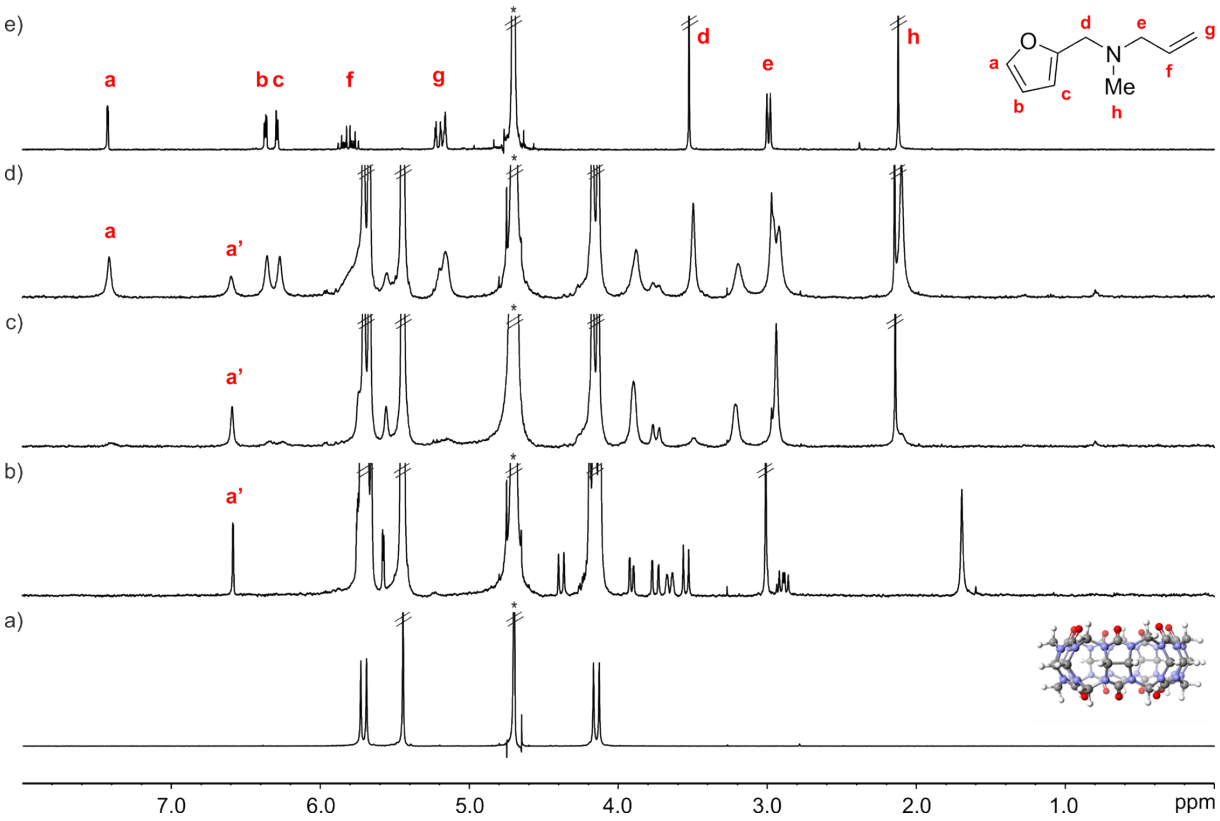

Figure S11. ^{1}H NMR spectra (400 MHz, D_2O, 298 K) of the titration experiment of **CB[7]** (5.0 mM) with **FA-1**: a) 0 equiv., b) 0.5 equiv., c) 1.05 equiv., d) 2.0 equiv. e) ^{1}H NMR spectrum of **FA-1**. Primed labels correspond to proton signals of bound molecules. *Residual solvent peak.

Table S1. Experimental chemical shifts of free (δ_{free}) and bound (δ_{bound}) **FA-1** in the **FA-1⊂CB[7]** complex, and complexation-induced shifts ($\Delta\delta$).

Signal	δ_{free} (ppm)	δ_{bound} (ppm)	$\Delta\delta$ (ppm)
a	7.52	6.69	-0.83
c	6.39	5.66	-0.73
d	3.62	3.99	+0.37
e	3.09	3.20	+0.11
g	5.29	3.92	-1.37

h	2.22	3.03	+0.81

III.3 Binding Studies of P-1 with CB[7] and DOSY Results

Pure **P-1** was titrated with **CB[7]** to confirm the formation of the **P-1⊂CB[7]** complex.

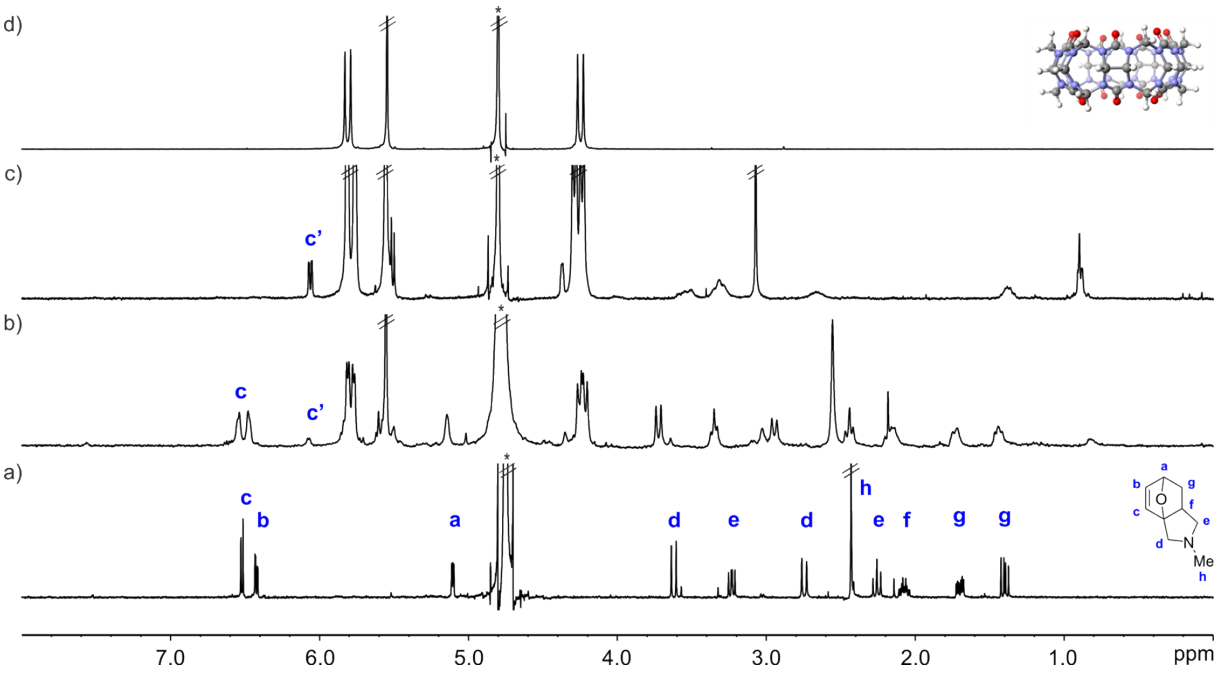

Figure S12. ^{1}H NMR spectra (400 MHz, D_2O, 298 K) of the titration experiment of **P-1** (5.0 mM) with **CB[7]**: a) 0 equiv., b) 0.25 equiv., c) 1.0 equiv. d) ^{1}H NMR spectrum of **CB[7]**. Primed labels correspond to proton signals of bound molecules. *Residual solvent peak.

The diagnostic signals of the **P-1⊂CB[7]** complex formed during the reaction of **FA-1** with **CB[7]** were identified by comparison of those obtained from an equimolar mixture of the DA cycloadduct **P-1** and **CB[7]**.

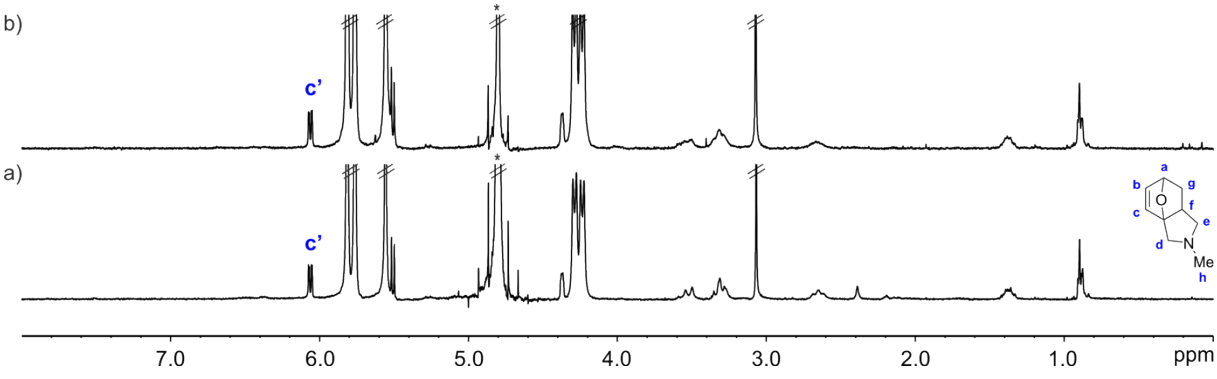

Figure S13. ^{1}H NMR spectra (400 MHz, D_2O, 298 K) of: a) **P-1⊂CB[7]** complex formed after 16 h of IMDA reaction of **FA-1** (5.0 mM) with **CB[7]** (1.0 equiv.), and b) equimolar mixture of the DA cycloadduct **P-1** (5.0 mM) with **CB[7]**. Primed labels correspond to proton signals of bound molecules. *Residual solvent peak.

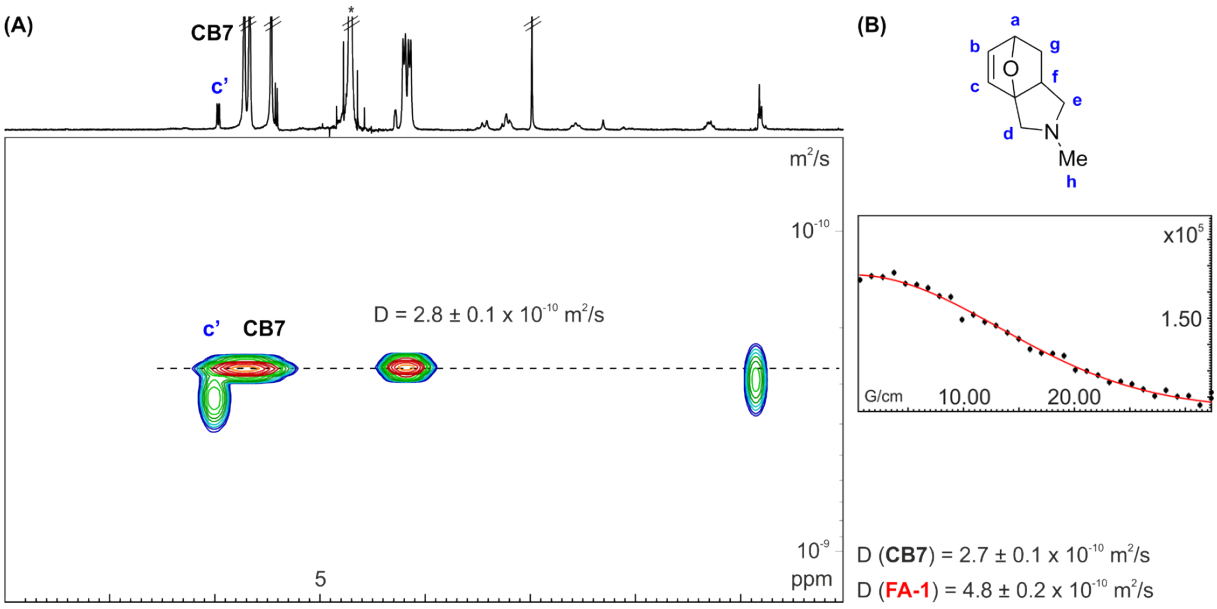

Figure S14. (A) ^{1}H pseudo 2D plot of DOSY (400 MHz, D_2O, 298 K, D20 = 0.15 s; P30 = 1.5 ms) of **CB[7]** (5.0 mM) with **P-1** (1.0 equiv.). (B) Fit of the decay of the signal of bound **P-1** (**c'**) to a mono-exponential function using Dynamics Center from Bruker. Errors are indicated as standard deviations. Diffusion coefficients for the free substrate **FA-1** and the free host **CB[7]** are provided for comparison (right bottom). Note the significant change on the diffusion coefficient constant experienced by the bound guest. As expected, the diffusion constant of bound CB[7] is not significantly changed. *Residual solvent peak.

III.4 Binding Studies of FA-2 with CB[7]

The formation of **FA-2⊂CB[7]** complex was demonstrated by ^{1}H NMR titration experiments. The addition of 1.0 equiv. of **FA-2** to a mM D_2O solution of **CB[7]** produced upfield shifts in the proton signals compared to the free amine. When 2.0 equiv. of **FA-2** were added, the proton signals of the amine broadened and moved downfield towards the chemical shifts of the free counterpart. These observations were indicative of the inclusion of **FA-2** in the hydrophobic cavity of **CB[7]** and the existence of a binding process showing intermediate chemical exchange dynamics on the chemical-shift timescale.

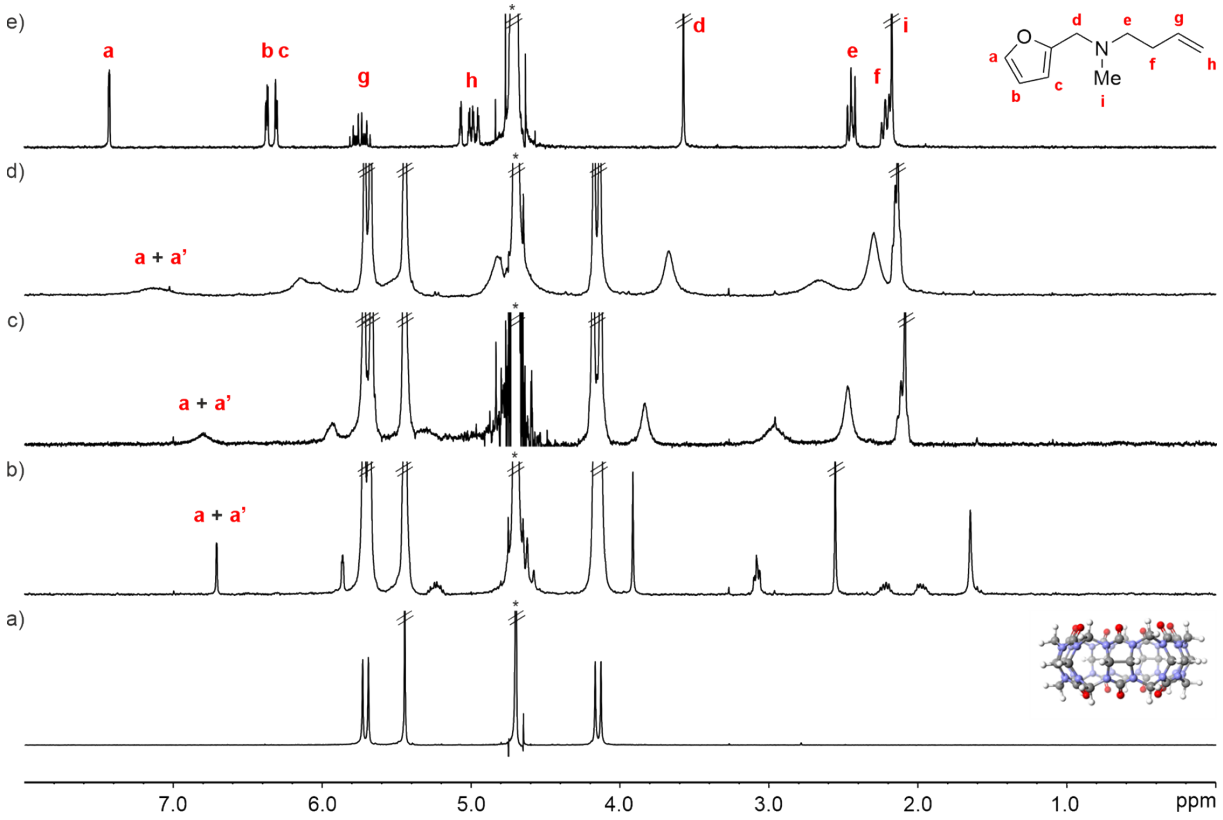

Figure S15. ^{1}H NMR spectra (400 MHz, D_2O, 298 K) of the titration experiment of **CB[7]** (5.0 mM) with **FA-2**: a) 0 equiv., b) 0.5 equiv., c) 1.0 equiv., d) 2.0 equiv. e) ^{1}H NMR spectrum of **FA-2**. Primed labels correspond to proton signals of bound molecules. *Residual solvent peak.

We used HypNMR2008 to fit the chemical shift changes experienced by **FA-2** and **CB[7]** to a 1:1 theoretical model. The obtained fit was good, supporting the assignment of a 1:1 stoichiometry to the formed complex. The fit returned a binding constant value K_a (**FA-2⊂CB[7]**) = (5.5 ± 0.5) x 10^3 M^{-1}.

III.5 Binding Studies of P-2 with CB[7] and DOSY Results

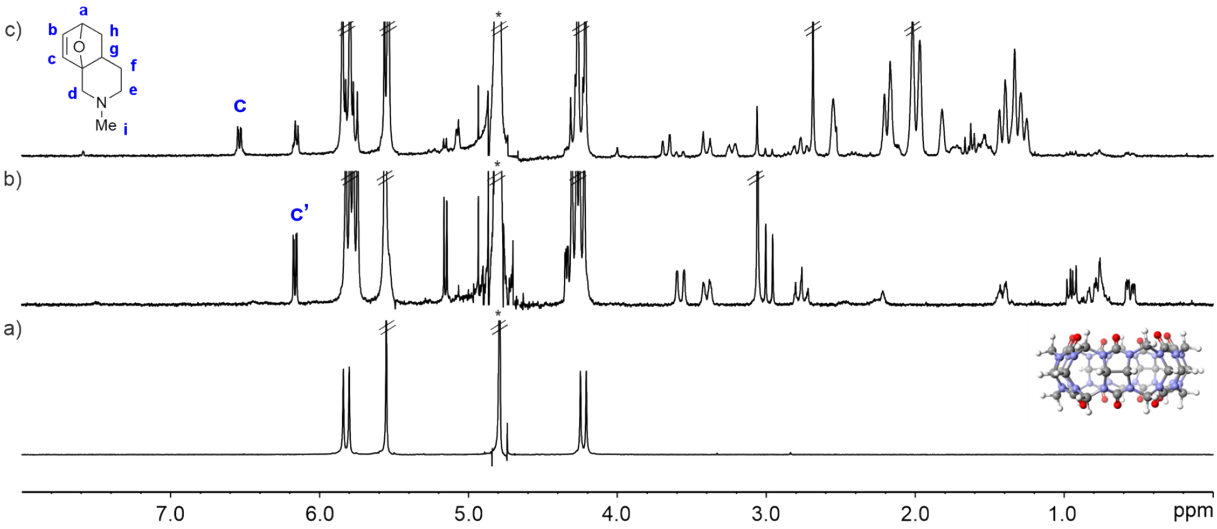

Figure S16. ^{1}H NMR spectra (400 MHz, D_2O, 298 K) of **CB[7]** (5.0 mM) with **P-2**: a) 0 equiv., b) 1.0 equiv. c) ^{1}H NMR spectrum of free and bound **P-2** (in a mixture with **CB[7]** and 2-adamantanone (**ADA**)). Primed labels correspond to proton signals of bound molecules. *Residual solvent peak.

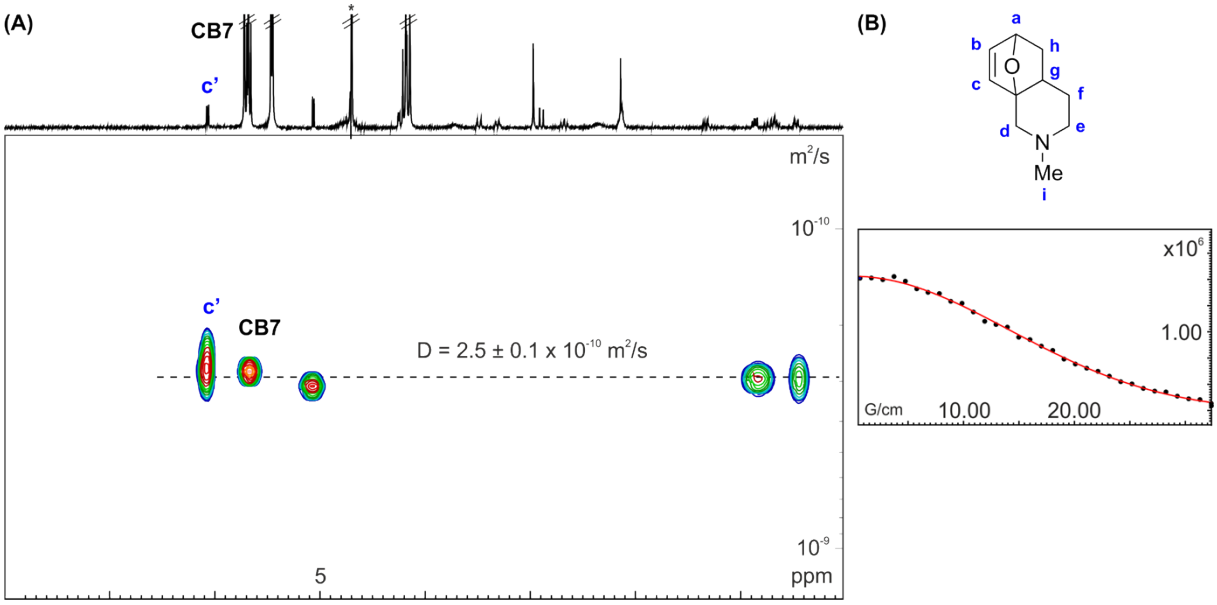

Figure S17. (A) ^{1}H pseudo 2D plot of DOSY (400 MHz, D_2O, 298 K, D20 = 0.15 s; P30 = 1.5 ms) of **CB[7]** (5.0 mM) with **P-2** (1.0 equiv.). (B) Fit of the decay of the signal of bound **P-2** (**c'**) to a mono-exponential function using Dynamics Center from Bruker. Errors are indicated as standard deviations. *Residual solvent peak.

III.6 Binding Studies of FA-1 with CB[8]

^{1}H NMR titration experiments showed that the binding process between **FA-1** and **CB[8]** displayed fast exchange dynamics on the ^{1}H NMR chemical-shift timescale.

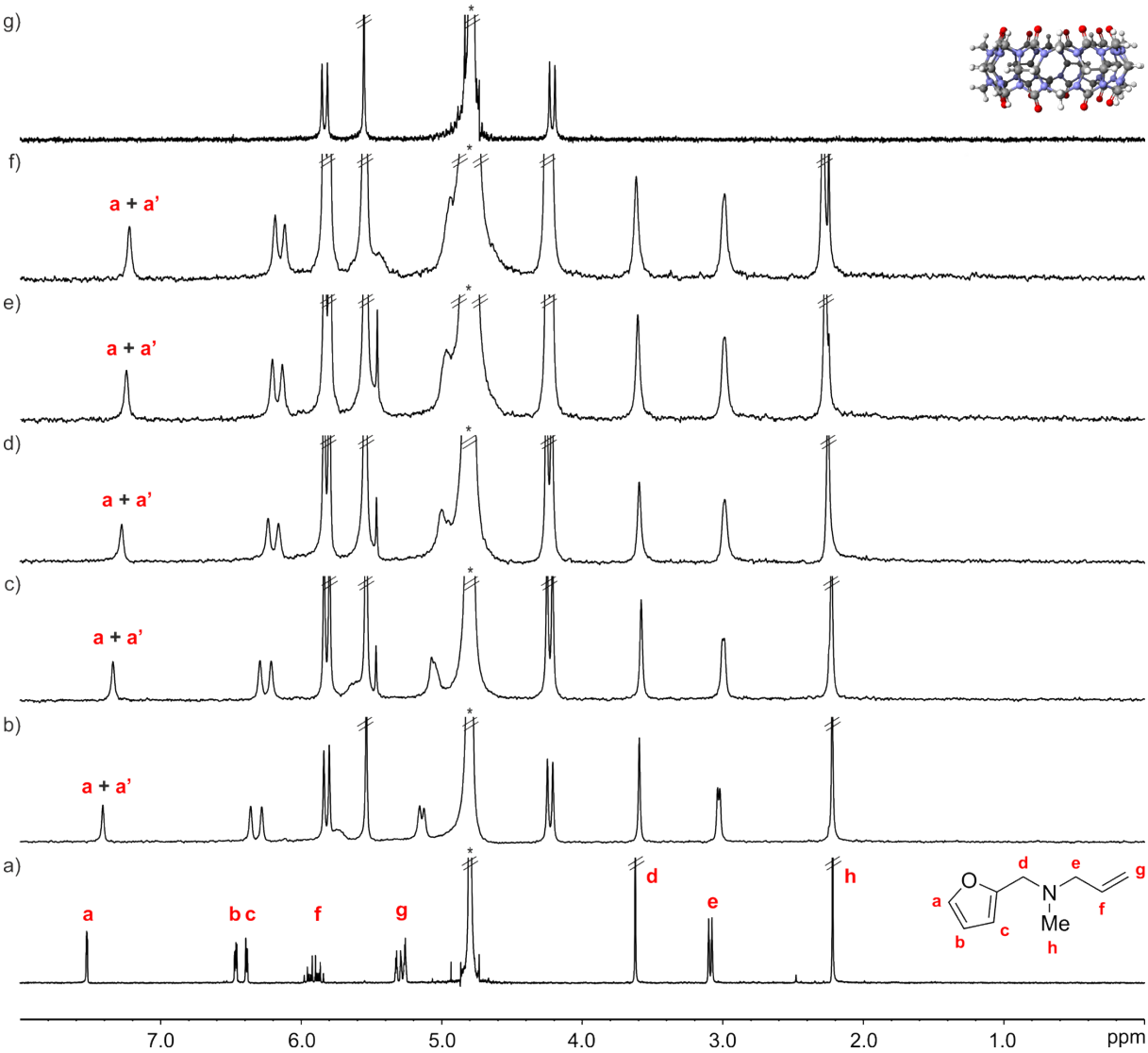

Figure S18. ^{1}H NMR spectra (400 MHz, D_2O, 298 K) of the titration experiment of **FA-1** (2.5 mM) with **CB[8]**: a) 0 equiv., b) 0.25 equiv., c) 0.5 equiv., d) 1.0 equiv., e) 1.25 equiv., f) 1.5 equiv. g) ^{1}H NMR spectrum of **CB[8]**. Primed labels correspond to proton signals of bound molecules. *Residual solvent peak.

We used HypNMR2008 to fit the chemical shift changes experienced by **FA-1** and **CB[8]** to a 1:1 theoretical model. The obtained fit was good, supporting the assignment of a 1:1

stoichiometry to the formed complex. The fit returned a binding constant value K_a (**FA-1⊂CB[8]**) = (1.1 ± 0.2) x 10^3 M^{-1}.

III.7 Binding Studies of FA-2 with CB[8]

^{1}H NMR titration experiments showed a binding process of **FA-2** with **CB[8]** that displayed fast exchange dynamics on the chemical-shift timescale.

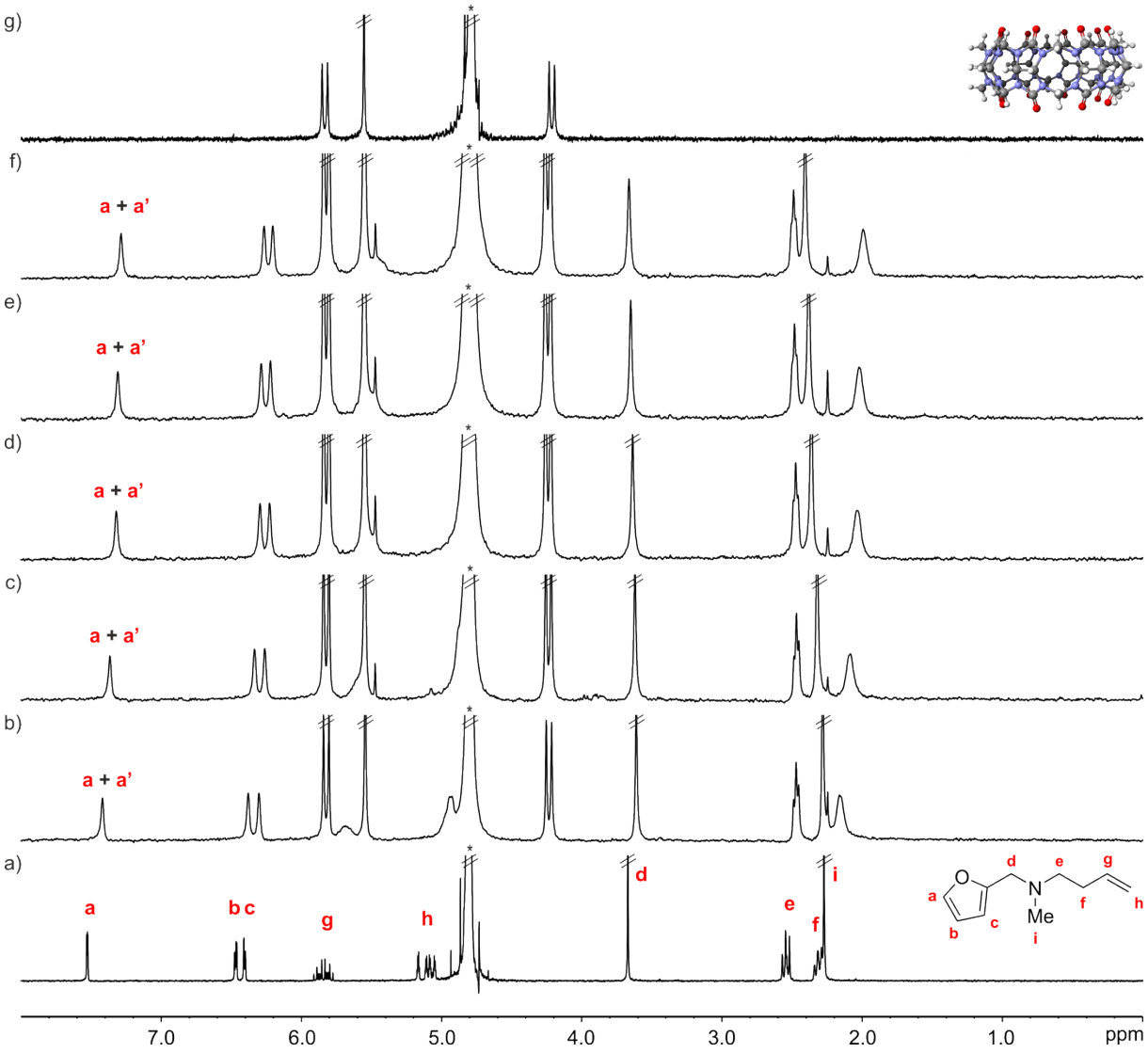

Figure S19. ^{1}H NMR spectra (400 MHz, D_2O, 298 K) of the titration experiment of **FA-2** (2.5 mM) with **CB[8]**: a) 0 equiv., b) 0.25 equiv., c) 0.5 equiv., d) 1.0 equiv., e) 1.25 equiv., f) 1.5 equiv. g) ^{1}H NMR spectrum of **CB[8]**. Primed labels correspond to proton signals of bound molecules. *Residual solvent peak.

We used HypNMR2008 to fit the chemical shift changes experienced by **FA-2** and **CB[8]** to a 1:1 theoretical model. The obtained fit was good, supporting the assignment of a 1:1 stoichiometry to the formed complex. The fit returned a binding constant value K_a (**FA-2⊂CB[8]**) = (1.8 ± 0.3) x 10^3 M^{-1}.

III.8 Isothermal Titration Calorimetry (ITC) Experiments of FA-1 and P-1 with CB[7]

Titrations were carried out in either H_2O or D_2O solutions by adding small aliquots of a solution of the guest (12 μL) from a computer controlled micro syringe into the solution of the host in the same solvent placed in the cell. The temperature was set to 298 K. Each experiment was performed at least in duplicate. The association constants (K_a) and enthalpy values were derived from the fit of the titration data to a 1:1 binding model implemented in the MicroCal ITC Data Analysis module. The results obtained are presented hereafter.

Table S2. Binding constant values (K_a) and thermodynamic parameters of the interaction of **FA-1** with **CB[7]** in H_2O or D_2O, and **P-1** with **CB[7]** in D_2O, as determined by ITC. Error values in K_a and ΔH are reported as standard deviations and propagated to ΔG and ΔS.

Guest⊂Host	Solvent	K_a [M^{-1}]	ΔG [kcal·mol^{-1}]	ΔH [kcal·mol^{-1}]	TΔS [kcal·mol^{-1}]
FA-1⊂CB[7]	H_2O	(2.2 ± 0.6) x 10^5	-7.3 ± 0.2	-11.9 ± 0.1	-4.6 ± 0.2
FA-1⊂CB[7]	D_2O	(8.1 ± 0.6) x 10^5	-8.1 ± 0.7	-14.8 ± 0.5	-6.7 ± 0.5
P-1⊂CB[7]	D_2O	(6.1 ± 0.3) x 10^5	-7.9 ± 0.6	-14.1 ± 0.5	-6.2 ± 0.4

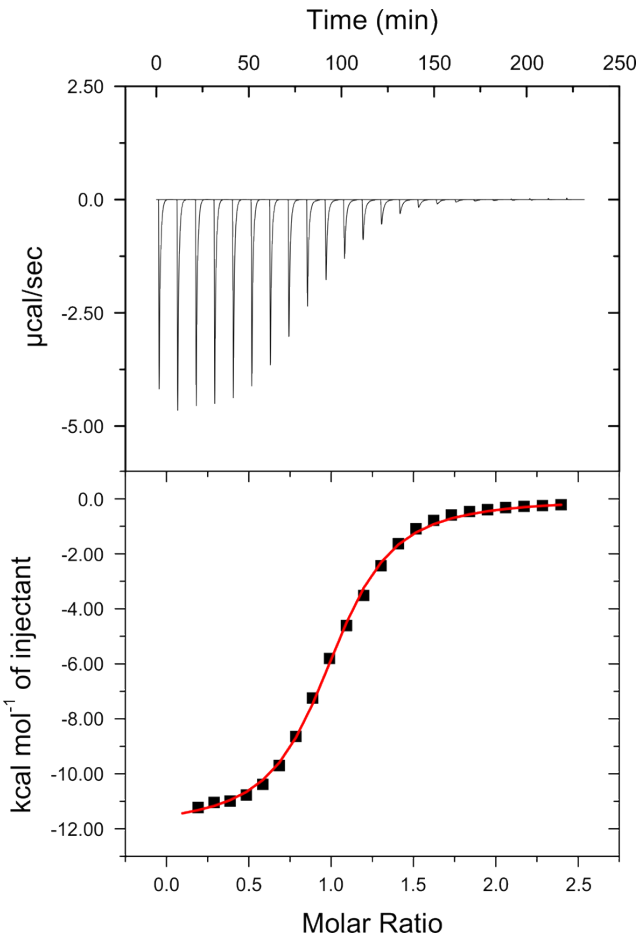

Figure S20. Trace shows raw data for the titration of guest into host: **FA-1** = 1.87 mM and **CB[7]** = 0.16 mM. Titration was performed at 298 K in H_2O. Binding isotherm of the calorimetric titration is shown on top. The enthalpy of binding for each injection is plotted versus the molar ratio of guest/host in the cell. The continuous line represents the least-squares-fit of the data to the "one set of sites" binding model (bottom).

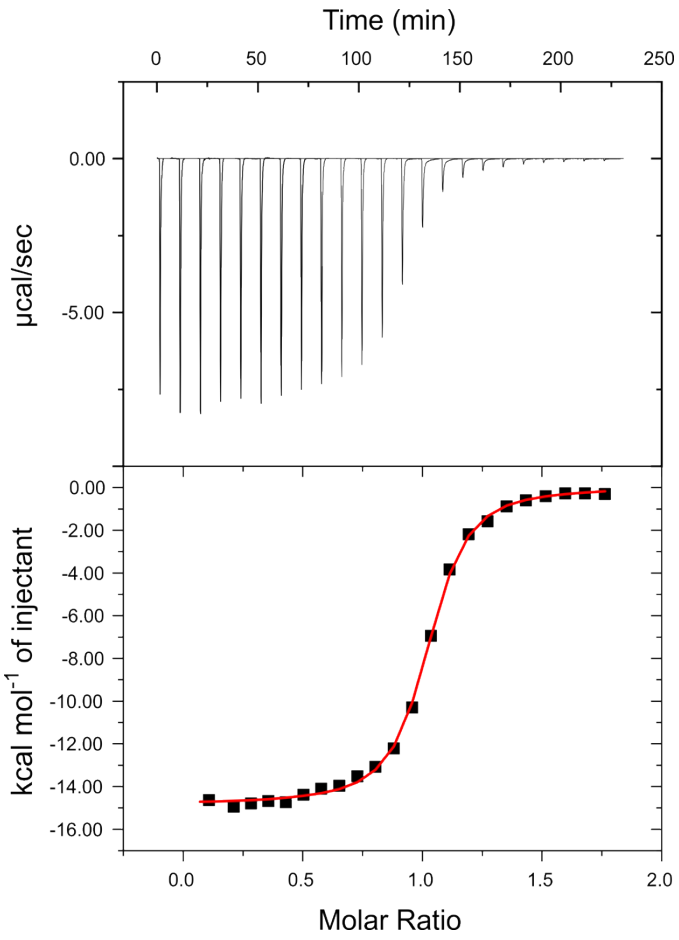

Figure S21. Trace shows raw data for the titration of guest into host: **FA-1** = 1.50 mM and **CB[7]** = 0.18 mM. Titration was performed at 298 K in D_2O. Binding isotherm of the calorimetric titration is shown on top. The enthalpy of binding for each injection is plotted versus the molar ratio of guest/host in the cell. The continuous line represents the least-squares-fit of the data to the "one set of sites" binding model (bottom).

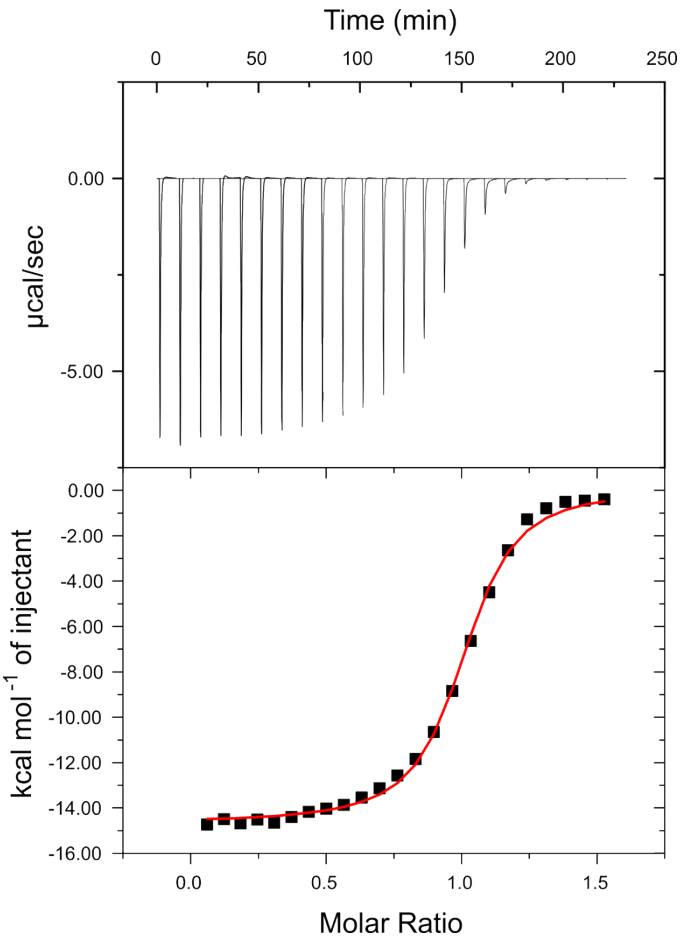

Figure S22. Trace shows raw data for the titration of guest into host: **P-1** = 1.30 mM and **CB[7]** = 0.18 mM. Titration was performed at 298 K in D_2O. Binding isotherm of the calorimetric titration is shown on top. The enthalpy of binding for each injection is plotted versus the molar ratio of guest/host in the cell. The continuous line represents the least-squares-fit of the data to the "one set of sites" binding model (bottom).

ITC experiments were not performed for guest **FA-2** with a binding constant value K_a (**FA-2⊂CB[7]**) = (5.5 ± 0.5) x 10^3 M^{-1}. Working with a Wiseman "*c*" parameter between 50-100, in order to obtain a good fitting of the experimental data to a sigmoidal curve, would requires receptor and guest concentrations that are not physically attainable.

III.9 Competitive Experiment of P-2⊂CB[7] with P-1

In order to estimate the binding constant value (K_a) of **P-2** with **CB[7]**, we performed a competitive experiment adding **P-1** (with a known binding constant value) to a preformed **P-2⊂CB[7]** complex.

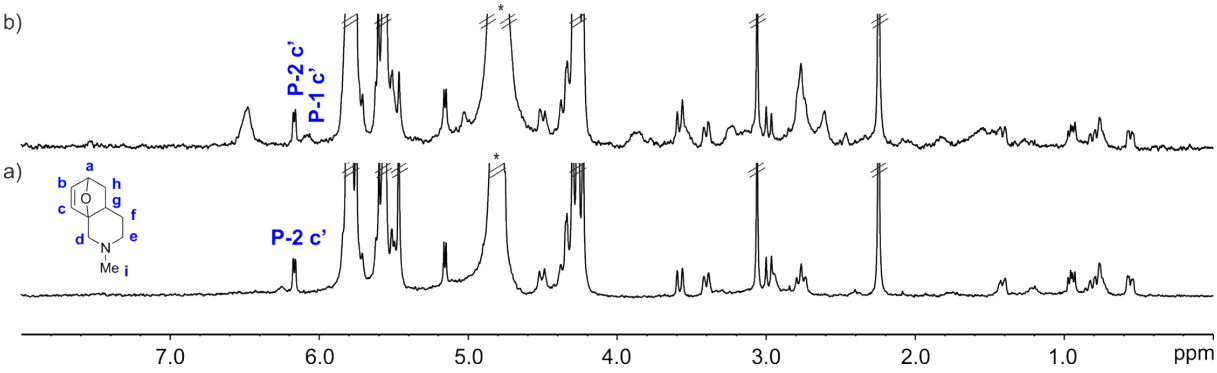

Figure S23. ^{1}H NMR spectra (400 MHz, D_2O, 298 K) of: a) **P-2⊂CB[7]** (1:1.25), and b) **P-2⊂CB[7]** (1:1.25, 0.00167 M) + **P-1** (1.0 equiv., 0.00167 M). Primed labels correspond to proton signals of bound molecules. *Residual solvent peak.

Based on the integration values of both complexes, we determined the ratio of their concentrations and calculated the concentrations of free **P-1** and **P-2** in the equilibrium. To do so, we assumed that the sum of the concentrations of bound **P-1** and **P-2** was similar to the initial concentration of **CB[7]** (2.09 mM). This assumption was based on the fact that the binding constants of the two complexes are larger than 10^4 M^{-1} and we were working at mM concentrations. The used math is described below. After determining the ratio of the stability constants of the complexes and knowing that K_a (**P-1⊂CB[7]**) was 6.1 x 10^5 M^{-1} (see Table S2) we determined K_a (**P-2⊂CB[7]**) to be 9.7 x 10^6 M^{-1}.

$$[P-1\subset CB[7]] + [P-2\subset CB[7]] \cong 2.09\ mM$$

$$\frac{[P-1\subset CB[7]]}{[P-2\subset CB[7]]} = 0.4$$

$$0.4\ x\ [P-2\subset CB[7]] + [P-2\subset CB[7]] = 2.09\ mM$$

$$[P-2\subset CB[7]] = 1.5\ mM$$

$$[P-1\subset CB[7]] = 0.4\ x\ [P-2\subset CB[7]] = 0.6\ mM$$

$$P_{total} = P_{free} + P_{bound}$$

$$[P-1]_{free} = 1.07\ mM;\ [P-2]_{free} = 0.17\ mM$$

$$\frac{K_a\,(P-1{\subset}CB[7])}{K_a\,(P-2{\subset}CB[7])} = \frac{[P-1{\subset}CB[7]]x[P-2_{free}]x[CB[7]]}{[P-2{\subset}CB[7]]x[P-1_{free}]x[CB[7]]} = \frac{0.6\ x\ 0.17}{1.5\ x\ 1.07} = 0.063$$

$$K_a\,(P-2{\subset}CB[7]) = 9.7\ x\ 10^6\ M^{-1}$$

III.10 Kinetic Characterization of the Complexes FA-1⊂CB[7] and P-1⊂CB[7]

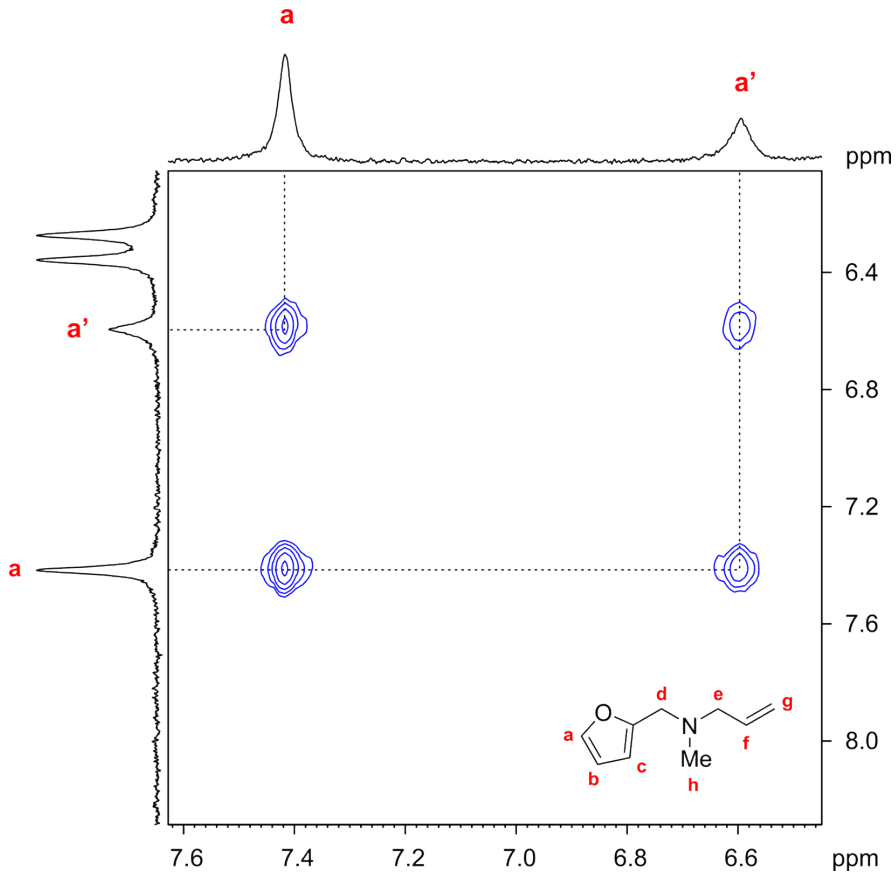

Figure S24. Selected region of the ^{1}H-^{1}H EXSY NMR spectrum (400 MHz, D_2O, 298 K, mixing time = 0.6 s) of **FA-1** (10 mM) and **CB[7]** (2:1 ratio). ^{1}H-^{1}H EXSY cross-peaks between free **FA-1** (signal a) and bound **FA-1** (signal a') acquired with three different mixing times (0.2, 0.4, and 0.6 s) were used to calculate the rate constants of the spin exchange (k_1 and k_{-1}). $k_{-1} = k_{off}$ (**FA-1⊂CB[7]**) = 1.1 s^{-1}.

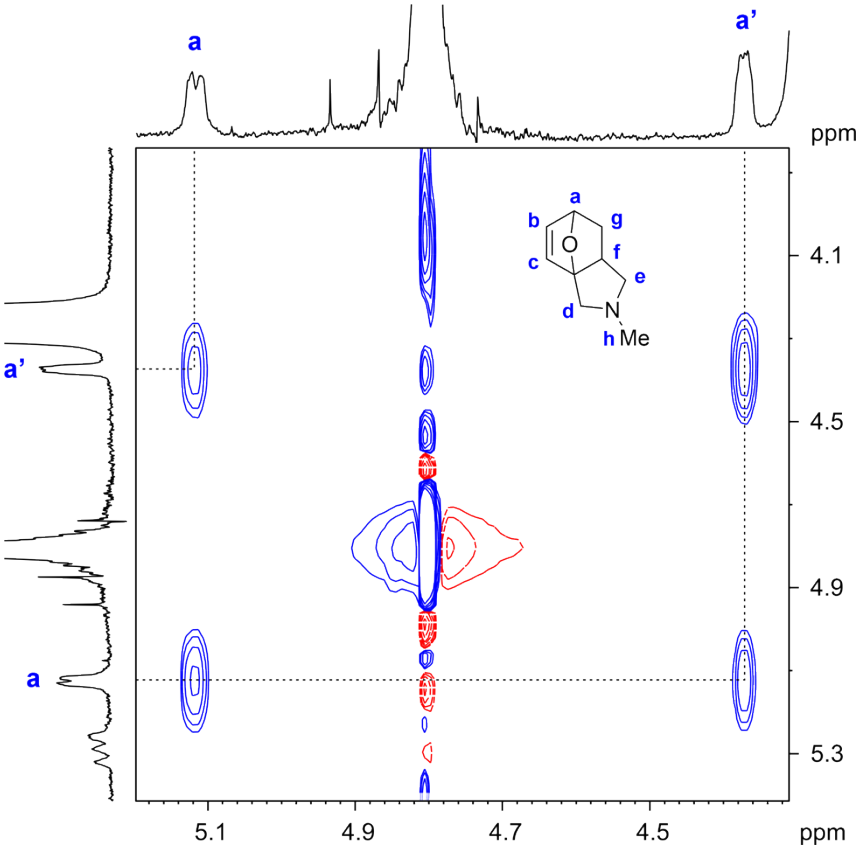

Figure S25. Selected region of the ^{1}H-^{1}H EXSY NMR spectrum (400 MHz, D_2O, 298 K, mixing time = 0.6 s) of **P-1** (10 mM) and **CB[7]** (2:1 ratio). ^{1}H-^{1}H EXSY cross-peaks between free **P-1** (signal a) and bound **P-1** (signal a') acquired with three different mixing times (0.2, 0.4, and 0.6 s) were used to calculate the rate constants of the spin exchange (k_1 and k_{-1}). $k_{-1} = k_{off}$ (**P-1⊂CB[7]**) = 1.2 s^{-1}.

IV. Theoretical Kinetic Models Used in the Fits and Simulations of the Reaction Profiles

Intramolecular Diels-Alder Cycloaddition Reaction of Tertiary Furfuryl Amines in the Absence of CB[*n*]s

The experimental kinetic data (concentration *vs.* time) obtained from the intramolecular Diels-Alder cycloaddition reaction of **FA-1** in D_2O were fit to a theoretical kinetic model using the Time Course or Parameter Estimation module of COPASI Software Version 4.25. We used the theoretical kinetic model shown below (Model 1) that corresponds to a first-order irreversible reaction.

Model 1

1) **FA-1** → **P-1**; k_{bulk}

k_{bulk} is the rate constant for the IMDA reaction of **FA-1** in the bulk solution. The experimental data were fit to the theoretical kinetic model returning the rate constant k_{bulk}.

In the case of **FA-2**, k_{bulk} was derived using the method of initial rates (*vide infra*).

Intramolecular Diels-Alder Cycloaddition Reaction of Tertiary Furfuryl Amines in the Presence of CB[*n*]s

The experimentally measured reaction profiles for the IMDA reactions of tertiary furfuryl amines (**FA**) in the presence of stoichiometric and catalytic amounts of **CB[*n*]s** were fit using the Time Course or Parameter Estimation modules of COPASI Software Version 4.25. We used the elaborated theoretical kinetic model shown below (Model 2), which considers: a) the unimolecular irreversible transformation of **FA** into **P** occurring in the bulk (background reaction) (equation 1), b) the reversible formation of the **FA⊂CB[*n*]** complex (equation 2), c) its irreversible transformation into the **P⊂CB[*n*]** counterpart (included IMDA reaction) (equation 3), and d) the reversible dissociation of the **P⊂CB[*n*]** complex into their binding partners (equation 4).

Model 2

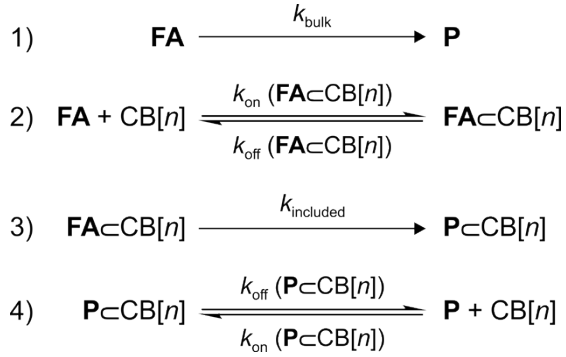

$k_{included}$ is the rate constant for the IMDA reaction of **FA** occurring in the inclusion complex. The experimental data were fit to the theoretical kinetic model returning the rate constant value for $k_{included}$.

The rate constant values k_{on} (**FA⊂CB[*n*]**), k_{off} (**FA⊂CB[*n*]**), k_{off} (**P⊂CB[*n*]**) and k_{on} (**P⊂CB[*n*]**) are pairwise related. Their ratio is derived from the determined/estimated equilibrium binding constants:

K_a (**FA⊂CB[*n*]**) = k_{on} (**FA⊂CB[*n*]**)/k_{off} (**FA⊂CB[*n*]**); K_a (**P⊂CB[*n*]**) = k_{on} (**P⊂CB[*n*]**)/k_{off} (**P⊂CB[*n*]**)

In turn, the binding constant values (K_a) were determined using ITC experiments or by fitting the chemical shift changes observed during the titration experiments to a 1:1 theoretical binding model. We used the HypNMR2008 software for the mathematical analyses of the titration data.

Whenever possible, we determined the values of the dissociation rate constants of the complexes, k_{off} (**FA⊂CB[*n*]**) and k_{off} (**P⊂CB[*n*]**), via ^{1}H-^{1}H EXSY experiments. The input data for the fit included the initial concentrations of the substrates **FA** and the containers **CB[*n*]s,** as well as the changes in concentration of the species used in the fit. We performed manual simulations of the reactions profiles and compared them with the experimental ones. The obtained values of the kinetic parameters were used as initial guesses in the optimization processes derived from the mathematical fit of the models to the experimentally measured speciation profiles.

Owing to the lack of reaction turnover, a simplified version of the elaborated model (*simplified Model 2*: equations 1-3) was used to fit the kinetic data in the case of **FA-2** with **CB[7]**, and also in the case of **FA-1** with **CB[8]**.

V. Kinetic Studies of FA-1 with CB[7]

V.1 General Procedure for Kinetic Experiments

A solution of the corresponding amine (10-20 mM) was prepared in D_2O. Subsequently, 0.3 mL of the solution were placed in an NMR tube. A solution of the corresponding cucurbit[*n*]uril (2-10 mM) was prepared in D_2O as well. CB[*n*] (0.3 mL) was added to the previous solution placed in the NMR tube. The samples were vortexed three times and inserted immediately into the NMR for analysis where ^1H NMR spectra (300 MHz or 400 MHz) were acquired. NMR spectra were acquired at different time intervals (see figure captions for details). Integration of the proton signals allowed the determination of the concentrations of the species in the IMDA reactions of **FA-1** and **FA-2**.

V.2 Kinetic Profiles

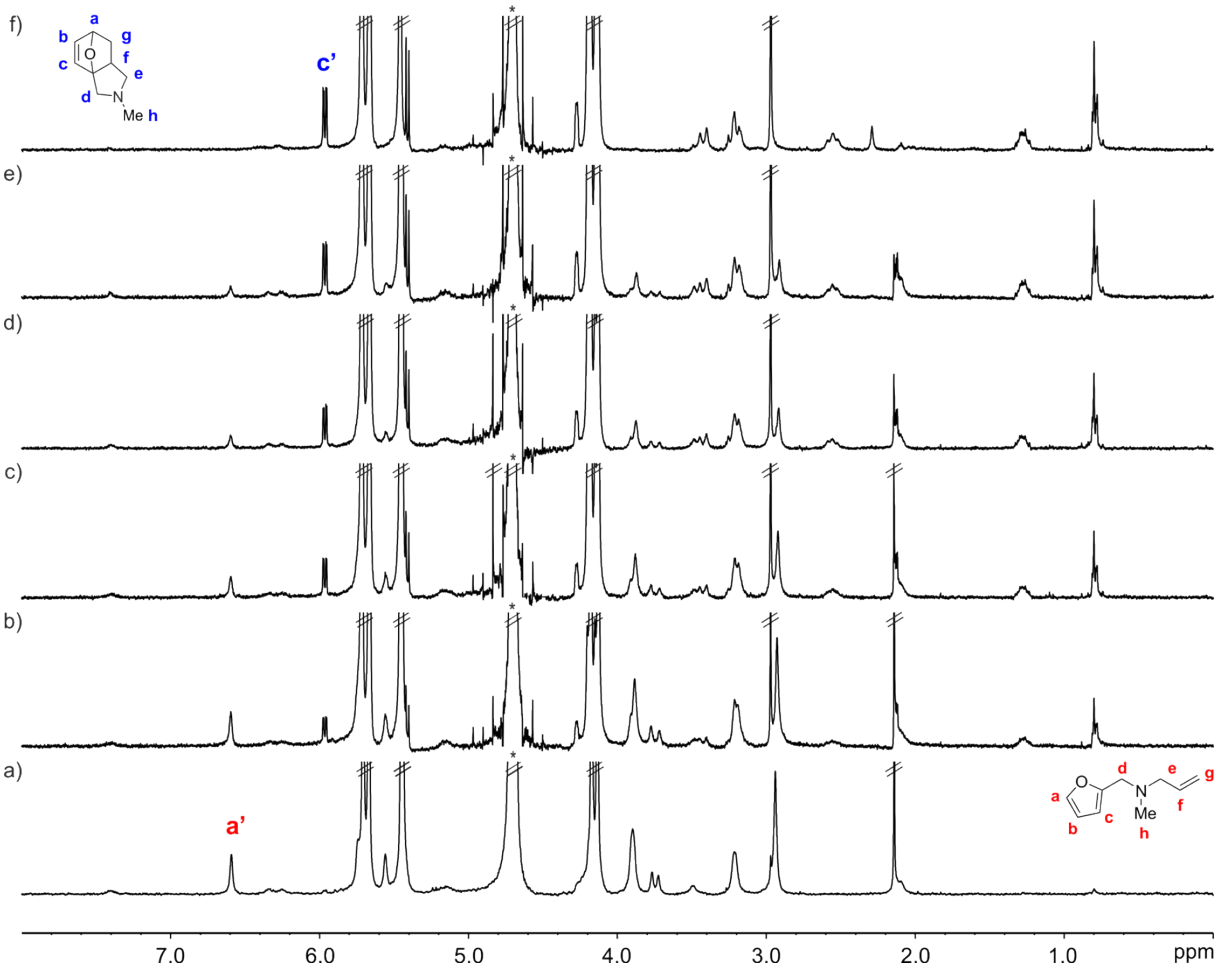

Figure S26. ^{1}H NMR spectra (300 MHz, D_2O, 298 K) of: a) **FA-1⊂CB[7]** (1:1, 0.005 M); and evolution of the IMDA reaction of **FA-1** (0.005 M) in the presence of **CB[7]** (1.0 equiv.) after: b) 2 h, c) 4 h, d) 6 h, e) 8 h, and f) 16 h. **FA-1** in red and **P-1** in blue. Primed labels correspond to proton signals of bound molecules. *Residual solvent peak.

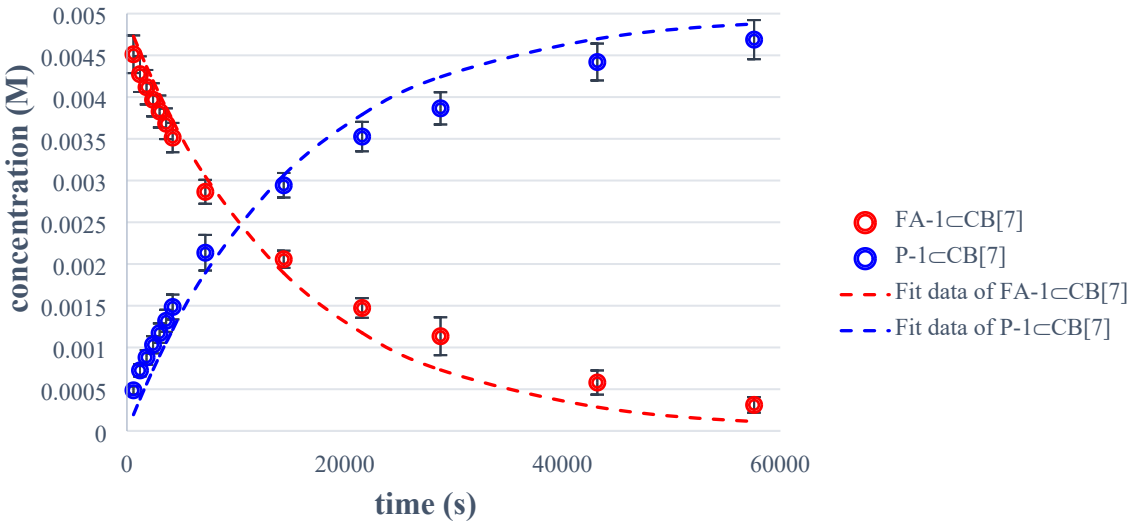

Figure S27. Plot of the concentrations (M) *vs.* time (s) for the IMDA reaction of **FA-1** (0.005 M) with **CB[7]** (1.0 equiv.) in D_2O at 298 K. Dashed lines represent the fit of the experimental data to the theoretical kinetic model 2 (Section IV). Error bars are standard deviations.

Table S3. Exchange rates of **FA-1⊂CB[7]** used for the fitting of the reaction profile represented in Figure S27 (**FA-1** (0.005 M) with **CB[7]** (1.0 equiv.) in D_2O at 298 K), and calculated rate constant value for the IMDA reaction ($k_{included}$). Error value in $k_{included}$ is reported as standard deviation.

Reaction	Constant
FA-1 → P-1	k_{bulk} = 1.1 x 10^{-7} s^{-1} [a]
FA-1 + CB[7] → FA-1⊂CB[7]	k_{on} (**FA-1⊂CB[7]**) = 8.9 x 10^5 $M^{-1}{\cdot}s^{-1}$ [b]
FA-1⊂CB[7] → FA-1 + CB[7]	k_{off} (**FA-1⊂CB[7]**) = 1.1 s^{-1} [c]
P-1⊂CB[7] → P-1 + CB[7]	k_{off} (**P-1⊂CB[7]**) = 1.2 s^{-1} [c]
P-1 + CB[7] → P-1⊂CB[7]	k_{on} (**P-1⊂CB[7]**) = 7.3 x 10^5 $M^{-1}{\cdot}s^{-1}$ [b]
FA-1⊂CB[7] → P-1⊂CB[7]	$k_{included}$ = (6.7 ± 0.3) x 10^{-5} s^{-1}

[a] Rate constant of the IMDA reaction of **FA-1** in the bulk at 298 K. [b] Calculated from $K_a = k_{on}/k_{off}$. K_a values were determined by ITC experiments. [c] Determined from ^{1}H-^{1}H EXSY experiments.

V.3 Competitive Displacement of the Bound Product

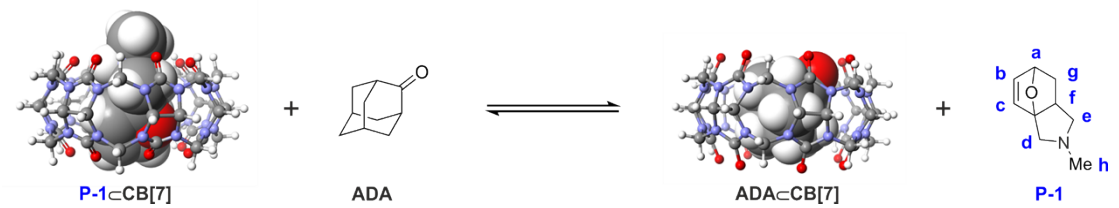

Scheme S1. Competitive binding equilibria of **P-1** and **ADA** with **CB[7]**.

The addition of 2-adamantanone (**ADA**) to the solution of **P-1⊂CB[7]** complex produced the immediate formation of the **ADA⊂CB[7]** counterpart. Concurrently, bound guest **P-1** was released to the bulk solution.

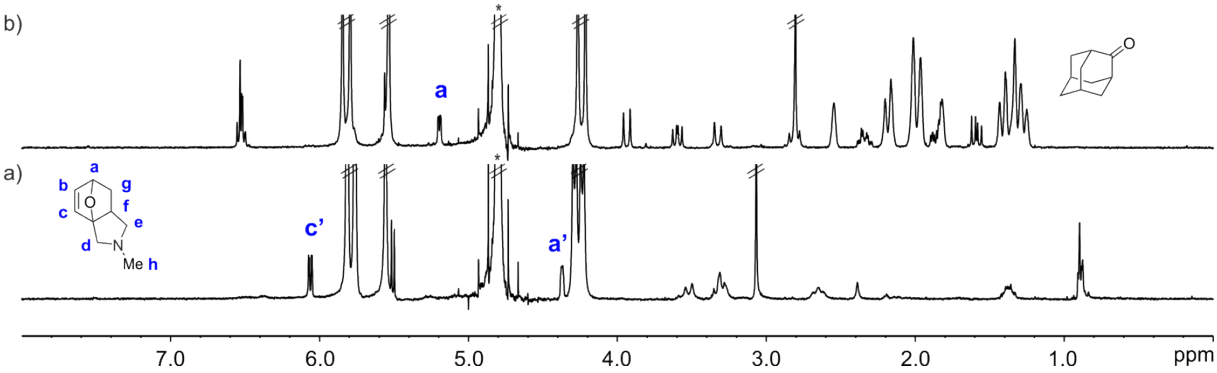

Figure S28. ^{1}H NMR spectra (300 MHz, D_2O, 298 K) of: a) **P-1⊂CB[7]** (1:1, 0.005 M), and b) addition of **ADA** to a). Primed labels correspond to proton signals of bound guest in **P-1⊂CB[7]**. *Residual solvent peak.

V.4 Control Experiment

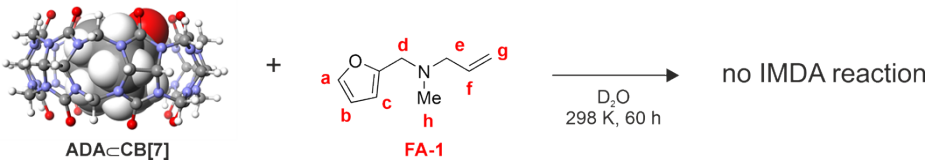

Scheme S2. Control experiment: addition of 1.0 equiv. of **FA-1** into a solution containing the preformed **ADA⊂CB[7]** complex.

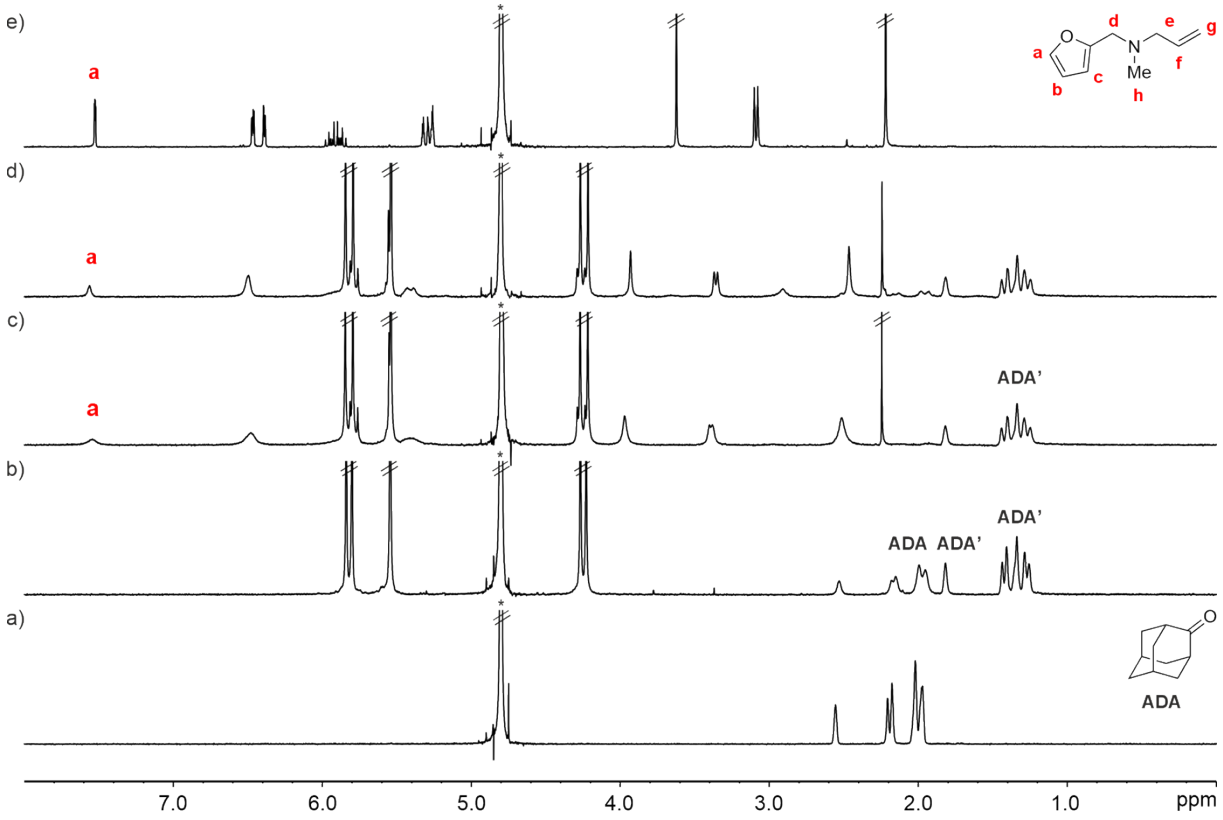

Figure S29. ^{1}H NMR spectra (300 MHz, D_2O, 298 K) of: a) **ADA**, b) **ADA⊂CB[7]** (2:1, 0.005 M), c) addition of **FA-1** (0.005 M) to **ADA⊂CB[7]** (1:1, 0.005 M), d) acquired after 60 h of spectrum c. e) ^{1}H NMR spectrum of **FA-1** (0.005 M). **FA-1** in red and **ADA** in black. Primed labels correspond to proton signals of bound molecules. *Residual solvent peak.

V.5 Kinetics upon Catalytic Amount of CB[7]

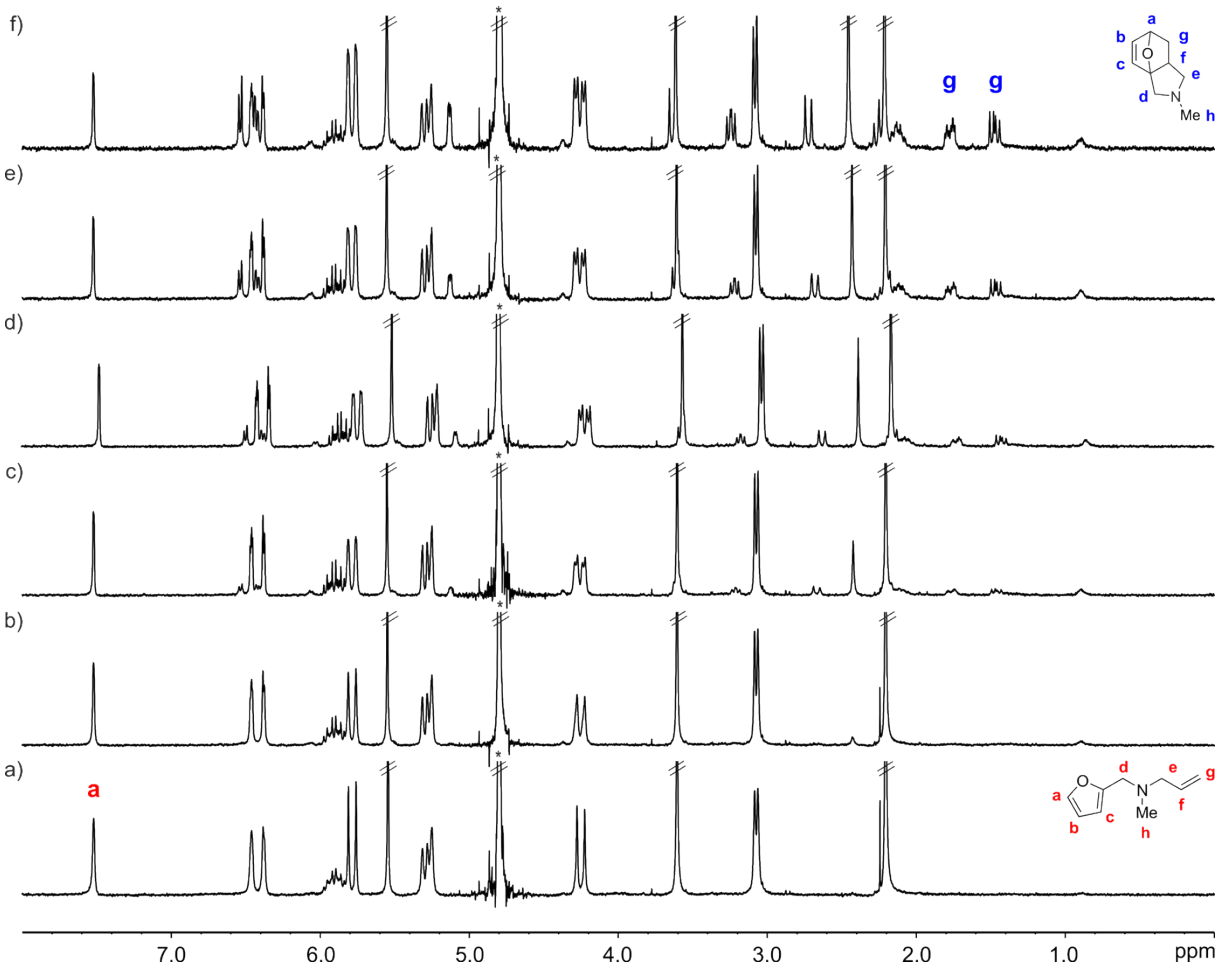

Figure S30. ^{1}H NMR spectra (300 MHz, D_2O, 298 K) of: a) **FA-1⊂CB[7]** (1:0.1, 0.01 M); and evolution of the IMDA reaction of **FA-1** (0.01 M) in the presence of **CB[7]** (0.1 equiv.) after: b) 8 h, c) 48 h, d) 84 h, e) 132 h, and f) 180 h. **FA-1** in red and **P-1** in blue. *Residual solvent peak.

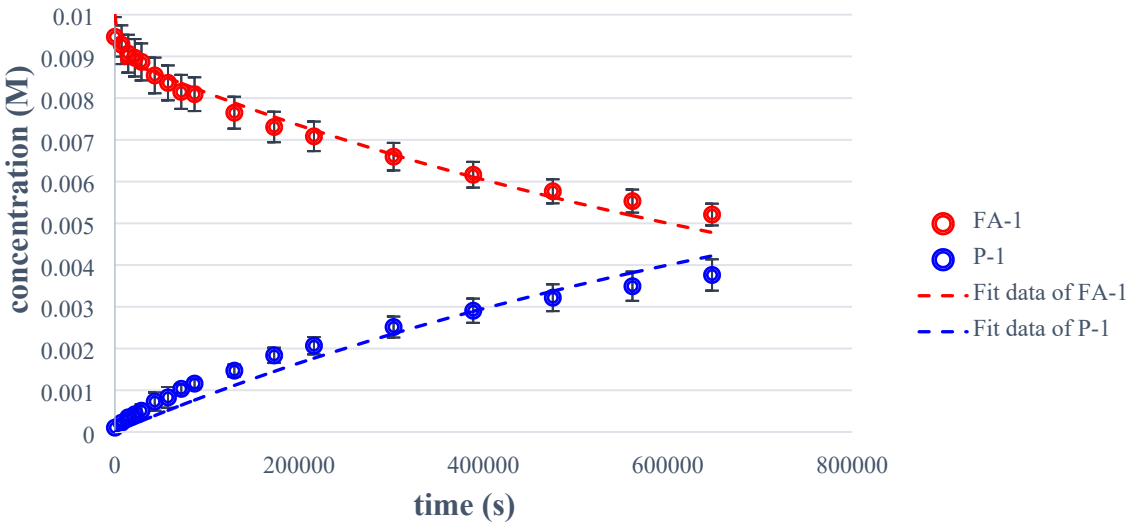

Figure S31. Plot of the concentrations (M) *vs.* time (s) for the IMDA reaction of **FA-1** (0.01 M) with **CB[7]** (0.1 equiv.) in D_2O at 298 K. Dashed lines represent the fit of the experimental data to the theoretical kinetic model 2 (Section IV). Error bars are standard deviations.

Table S4. Rate constant values and exchange rates of **FA-1⊂CB[7]** and **P-1⊂CB[7]** used for the fitting of the reaction profile represented in Figure S31 (**FA-1** (0.01 M) with **CB[7]** (0.1 equiv.) in D_2O at 298 K), and calculated rate constant value for the IMDA reaction ($k_{included}$). Error value in $k_{included}$ is reported as standard deviation.

Reaction	Constant
FA-1 → P-1	k_{bulk} = 1.1 x 10^{-7} s^{-1} [a]
FA-1 + CB[7] → FA-1⊂CB[7]	k_{on} (**FA-1⊂CB[7]**) = 8.9 x 10^5 $M^{-1}{\cdot}s^{-1}$ [b]
FA-1⊂CB[7] → FA-1 + CB[7]	k_{off} (**FA-1⊂CB[7]**) = 1.1 s^{-1} [c]
P-1⊂CB[7] → P-1 + CB[7]	k_{off} (**P-1⊂CB[7]**) = 1.2 s^{-1} [c]
P-1 + CB[7] → P-1⊂CB[7]	k_{on} (**P-1⊂CB[7]**) = 7.3 x 10^5 $M^{-1}{\cdot}s^{-1}$ [b]
FA-1⊂CB[7] → P-1⊂CB[7]	$k_{included}$ = (8.3 ± 0.2) x 10^{-6} s^{-1}

[a] Rate constant of the IMDA reaction of **FA-1** in the bulk at 298 K. [b] Calculated from $K_a = k_{on}/k_{off}$. K_a values were determined by ITC experiments. [c] Determined from ^1H-^1H EXSY experiments.

V.6 Determination of Activation Parameters under Standard Reaction Conditions

The IMDA cycloaddition reactions were run at least in duplicate at 298 K, 308 K, 318 K, and 328 K. The rate constants were determined for each temperature in the presence and absence

of the container (the kinetic profiles for the reactions performed with **CB[7]** are shown henceforward).

Table S5. Rate constant values determined by fitting the experimental data to the theoretical kinetic model with the Time Course and Parameter Estimation modules of COPASI Software Version 4.25. Error values in k_{bulk} (Model 1) and $k_{included}$ (Model 2) are reported as standard deviations.

System	T (K)	$k_{included}$ (s^{-1})	System	T (K)	k_{bulk} (s^{-1})
FA-1⊂CB[7]	298	(6.7 ± 0.3) x 10^{-5}	**FA-1**	298	(1.1 ± 0.1) x 10^{-7}
FA-1⊂CB[7]	308	(3.5 ± 0.1) x 10^{-4}	**FA-1**	308	(5.9 ± 0.2) x 10^{-7}
FA-1⊂CB[7]	318	(1.1 ± 0.1) x 10^{-3}	**FA-1**	318	(1.1 ± 0.1) x 10^{-6}
FA-1⊂CB[7]	328	(2.9 ± 0.1) x 10^{-3}	**FA-1**	328	(1.8 ± 0.1) x 10^{-6}

Plotting ln(k/T) vs. 1/T (Eyring plot) resulted in a straight line (Figure S32), and fitting data to eq. 1 provided the activation enthalpy and entropy ($\Delta H^{\neq}$, $\Delta S^{\neq}$). The linearity of the curve support that the kinetic parameters can be considered as constants in the studied range of temperatures.

$$\ln\frac{k}{T} = -\frac{\Delta H^{\neq}}{R}\frac{1}{T} + \frac{\Delta S^{\neq}}{R} + \ln\frac{k_B}{h} \qquad \text{(eq. 1)}$$

In eq. 1, k_B: Boltzmann constant (1.38 x 10^{-23} J·K^{-1}); h: Planck constant (6.62 x 10^{-34} J·s); and R: gas constant (1.987 cal·mol^{-1}·K^{-1}).

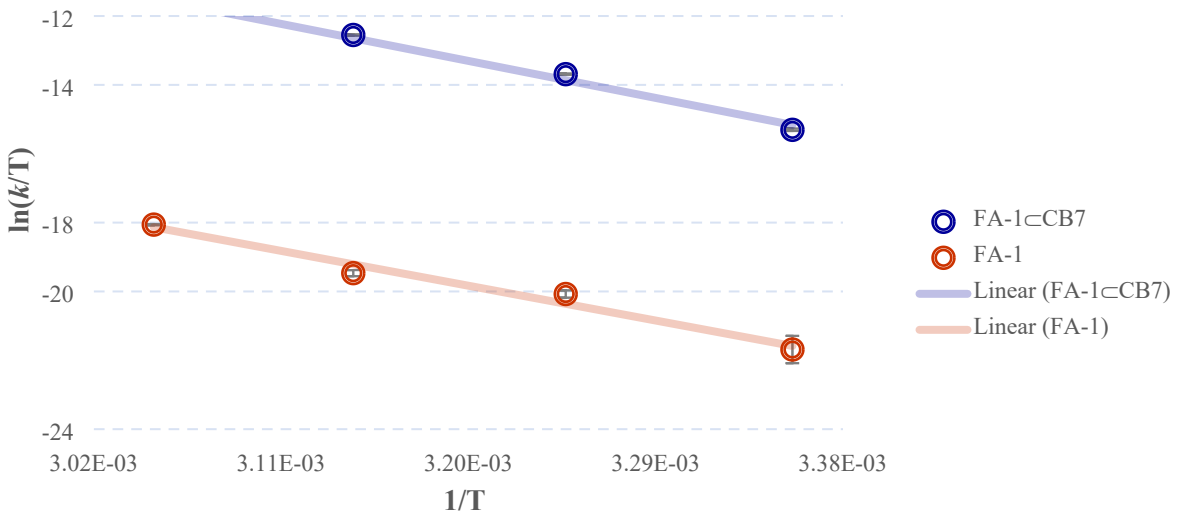

Figure S32. Eyring plots for **FA-1⊂CB[7]** (1:1, 0.005 M), and **FA-1** (0.005 M) in D_2O. Error bars are standard deviations.

The activation parameters of the IMDA reactions of **FA-1⊂CB[7]** (1:1, 0.005 M), and **FA-1** (0.005 M) in D_2O are summarized in the following table:

Table S6. Activation parameters of the IMDA reactions of **FA-1⊂CB[7]** (1:1, 0.005 M), and **FA-1** (0.005 M) in D_2O. Error values in $\Delta H^{\neq}$ and $\Delta S^{\neq}$ are reported as standard deviations and propagated to $\Delta G^{\neq}$.

System	$\Delta H^{\neq}$ [kcal·mol^{-1}]	$\Delta S^{\neq}$ [cal·mol^{-1}·K^{-1}]	$T\Delta S^{\neq}$ [kcal·mol^{-1}] [a]	$\Delta G^{\neq}$ [kcal·mol^{-1}] [a]
FA-1⊂CB[7]	23.7 ± 0.1	2.3 ± 0.4	0.7 ± 0.1	23.0 ± 0.2
FA-1	22.3 ± 0.5	-15.2 ± 1.6	-4.5 ± 0.5	26.9 ± 0.2

[a] 298 K.

Kinetic profiles for the reactions performed with **FA-1⊂CB[7]** (1:1, 0.005 M) at 308 K, 318 K and 328 K:

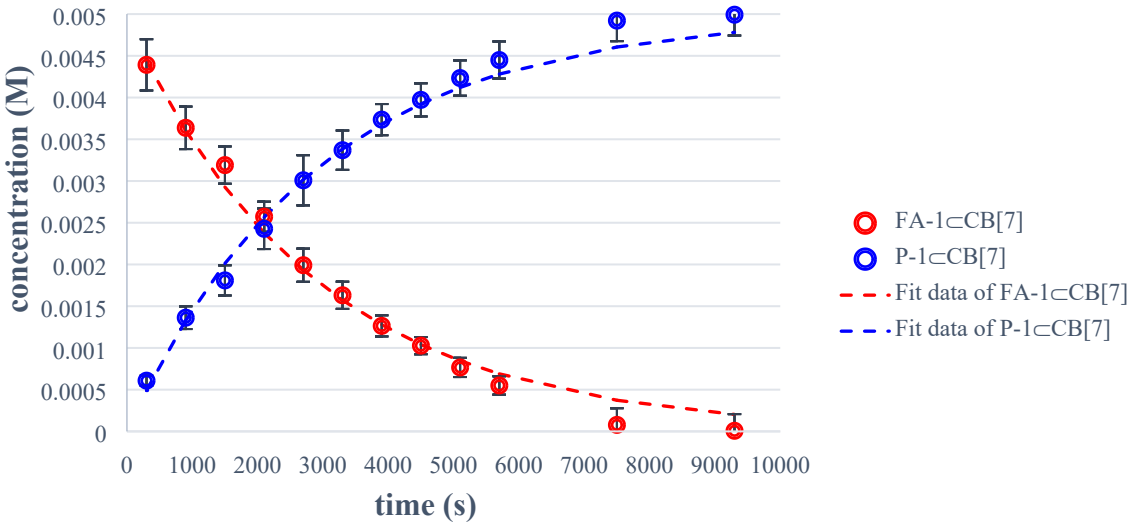

Figure S33. Plot of the concentrations (M) *vs.* time (s) for the IMDA reaction of **FA-1** (0.005 M) with **CB[7]** (1.0 equiv.) in D_2O at 308 K. Dashed lines represent the fit of the experimental data to the theoretical kinetic model 2 (Section IV). Error bars are standard deviations.

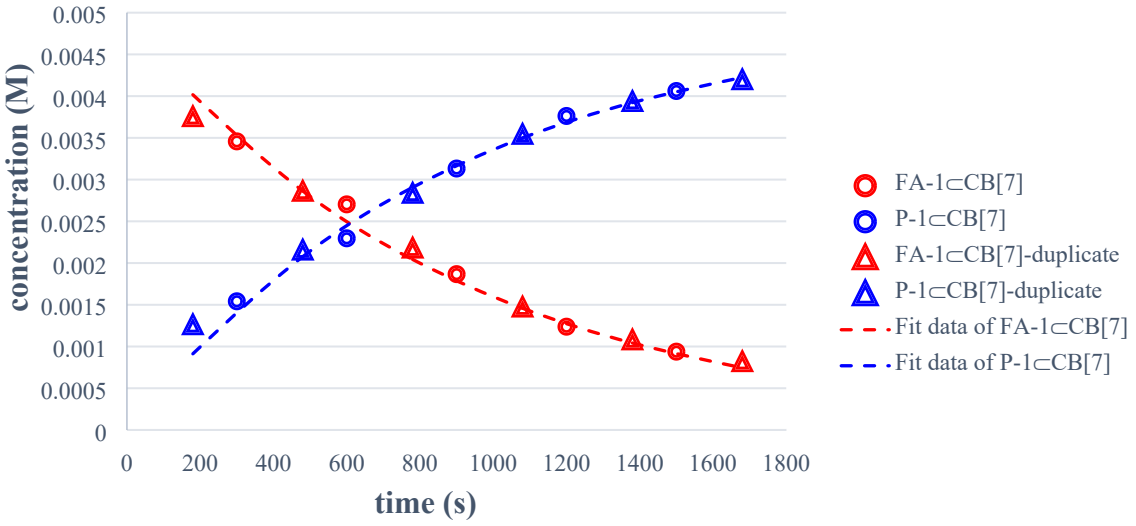

Figure S34. Plot of the concentrations (M) *vs.* time (s) for the IMDA reaction of **FA-1** (0.005 M) with **CB[7]** (1.0 equiv.) in D_2O at 318 K. The experimental data shown are the average of two duplicate experiments. Dashed lines represent the fit of the experimental data to the theoretical kinetic model 2 (Section IV). Error of $k_{included}$ is reported as standard deviation.

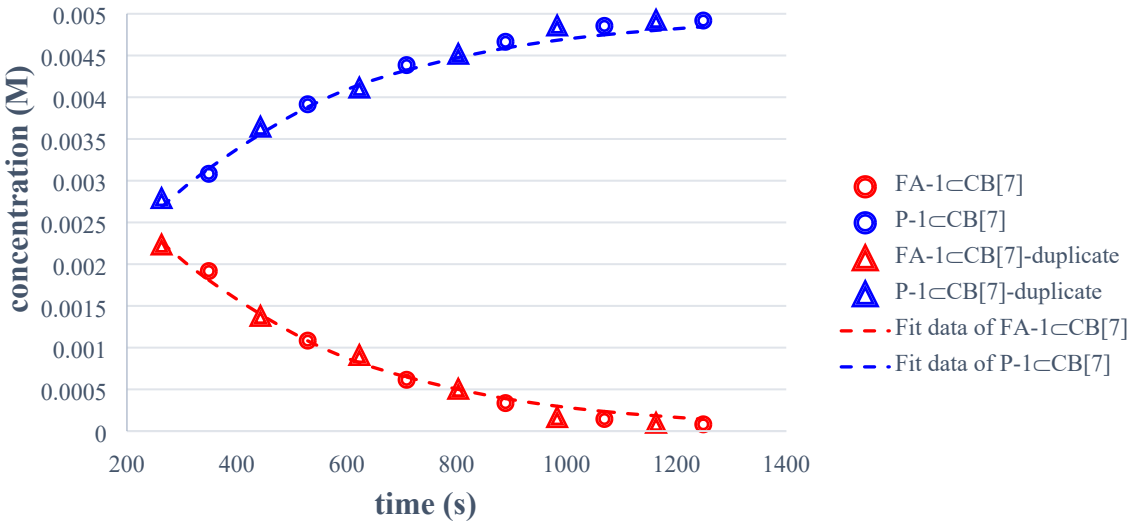

Figure S35. Plot of the concentrations (M) *vs.* time (s) for the IMDA reaction of **FA-1** (0.005 M) with **CB[7]** (1.0 equiv.) in D_2O at 328 K. The experimental data shown are the average of two duplicate experiments. Dashed lines represent the fit of the experimental data to the theoretical kinetic model 2 (Section IV). Error of $k_{included}$ is reported as standard deviation.

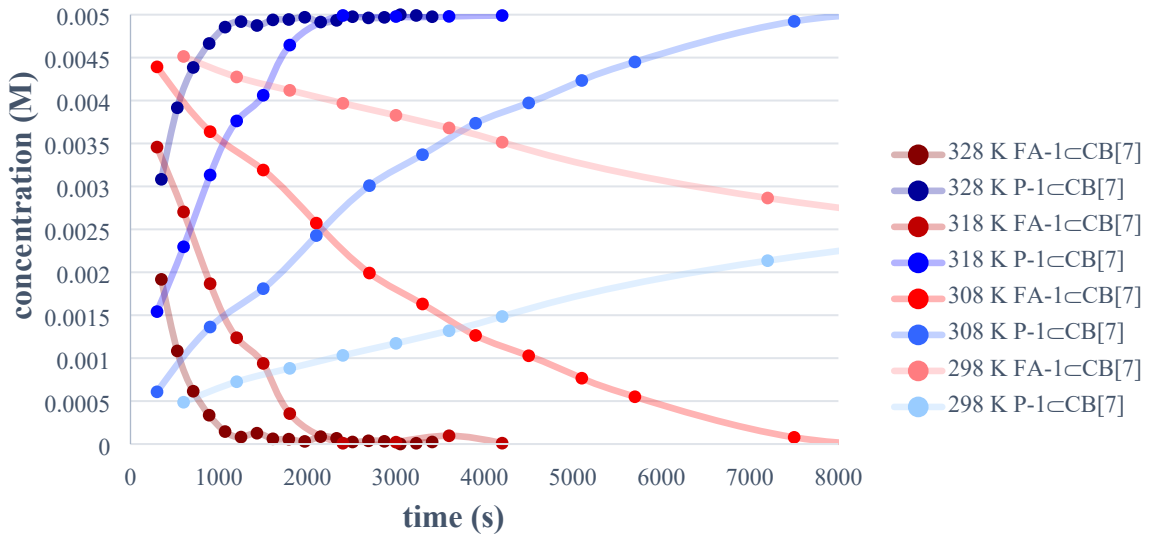

Figure S36. Experimentally measured reaction concentration profiles [concentration (M) *vs.* time (s)] for the IMDA reaction of **FA-1** (0.005 M) with **CB[7]** (1.0 equiv.) in D_2O at different temperatures.

V.7 Derivation of the Rate Law

We performed multiple reactions at different concentrations of **FA-1** and **CB[7].** We wanted to verify the correctness of using a unimolecular first order reaction rate law, based exclusively on the concentration of the inclusion complex, in deriving approximate value of rate constant from the initial rates of the included IMDA reactions. The effect of the changes in concentrations with respect to the initial reaction rate showed a kinetic saturation behavior typical of enzymes. We concluded that when working under saturation kinetic conditions [**FA-1**] = [**CB[7]**] ≥ 5 mM, the kinetic activity only depended on the concentration of the catalytic complex **FA-1⊂CB[7]**.

Table S7. Initial rates of the IMDA reactions of **FA-1⊂CB[7]** in D_2O. Error values are reported as standard deviations.

Ratio c (FA-1) : c (CB[7])	c (FA-1) [M] [a]	c (CB[7]) [M] [a]	c (FA-1 ⊂ CB[7]) [M] [b]	initial rate [M·s^{-1}] [c]
1:1	0.0050	0.0050	0.0050	(7.5 ± 0.3) x 10^{-7}
1:1	0.0025	0.0025	0.0025	(3.6 ± 0.8) x 10^{-7}
2:1	0.0100	0.0050	0.0050	(7.1 ± 0.4) x 10^{-7}
1:2	0.0025	0.0050	0.0025	(3.3 ± 0.3) x 10^{-7}

[a] Initial concentration. [b] Since the association constant of the complex **FA-1⊂CB[7]** in D_2O is > 10^4 M^{-1} (K_a = (8.1 ± 0.6) x 10^5 M^{-1}), we assume its quantitative formation at the concentrations used to perform the reactions. [c] To obtain the initial rate, we performed measurements of product concentrations when the reaction has evolved less than 10%. The data points were used to calculate a regression line with the y intercept of the line set to 0. The returned slope was used as the initial rate value.

VI. Kinetic Studies of FA-2 with CB[7]

VI.1 Kinetic Profiles

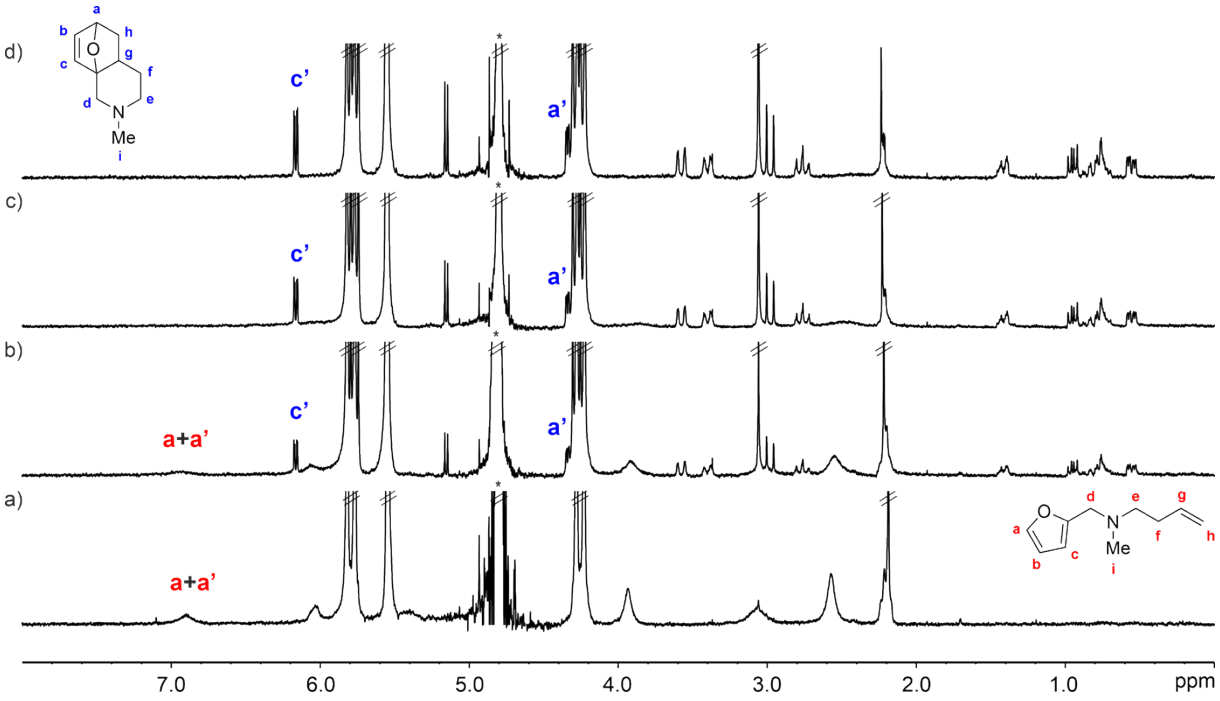

Figure S37. ^{1}H NMR spectra (300 MHz, D_2O, 298 K) of: a) **FA-2⊂CB[7]** (1:1, 0.005 M); and evolution of the IMDA reaction of **FA-2** (0.005 M) in the presence of **CB[7]** (1.0 equiv.) after: b) 2 h, c) 6 h, and d) 10 h. **FA-2** in red and **P-2** in blue. Primed labels correspond to proton signals of bound molecules. *Residual solvent peak.

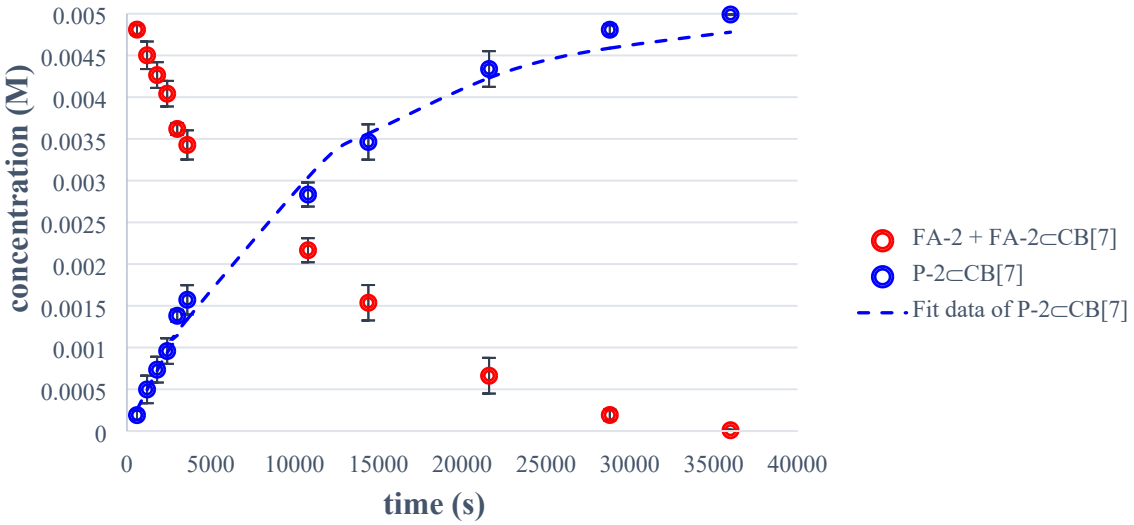

Figure S38. Plot of the concentrations (M) *vs.* time (s) for the IMDA reaction of **FA-2** (0.005 M) with **CB[7]** (1.0 equiv.) in D_2O at 298 K. Dashed line represents the fit of the experimental data to the simplified theoretical kinetic model 2 (Section IV). Error bars are standard deviations.

Table S8. Exchange rate constants of the **FA-2⊂CB[7]** complex used for the fitting of the reaction profile represented in Figure S38 (**FA-2** (0.005 M) with **CB[7]** (1.0 equiv.) in D_2O at 298 K), and calculated rate constant value for the IMDA reaction ($k_{included}$). Error value in $k_{included}$ is reported as standard deviation.

Reaction	Constant
FA-2 → P-2	k_{bulk} = 1.0 x 10^{-8} s^{-1} [a]
FA-2 + CB[7] → FA-2⊂CB[7]	k_{on} (**FA-2⊂CB[7]**) = 5.5 x 10^{3} $M^{-1}{\cdot}s^{-1}$ [b]
FA-2⊂CB[7] → FA-2 + CB[7]	k_{off} (**FA-2⊂CB[7]**) = 1.0 s^{-1} [b]
FA-2⊂CB[7] → P-2⊂CB[7]	$k_{included}$ = (1.2 ± 0.1) x 10^{-4} s^{-1}

[a] Estimated rate constant of the IMDA reaction of **FA-2** in the bulk at 298 K. [b] Estimated from K_a = k_{on}/k_{off} = 5.5 x 10^3 M^{-1} and assuming k_{off} = 1.0 s^{-1}.

VI.2 Competitive Displacement of the Bound Product

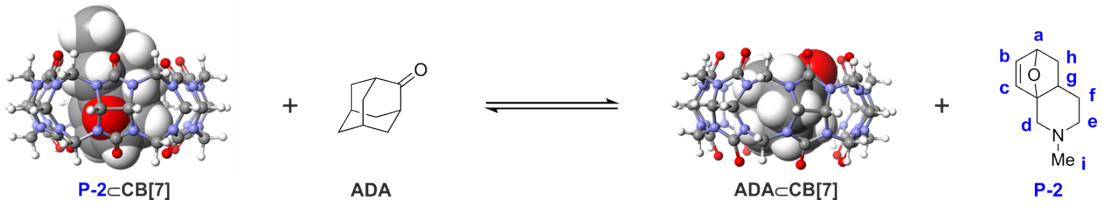

Scheme S3. Competitive binding equilibria of **P-2** and **ADA** with **CB[7]**.

The addition of 2-adamantanone (**ADA**) to the solution of **P-2⊂CB[7]** complex produced the immediate formation of the **ADA⊂CB[7]** counterpart. Concurrently, bound guest **P-2** was released to the bulk solution.

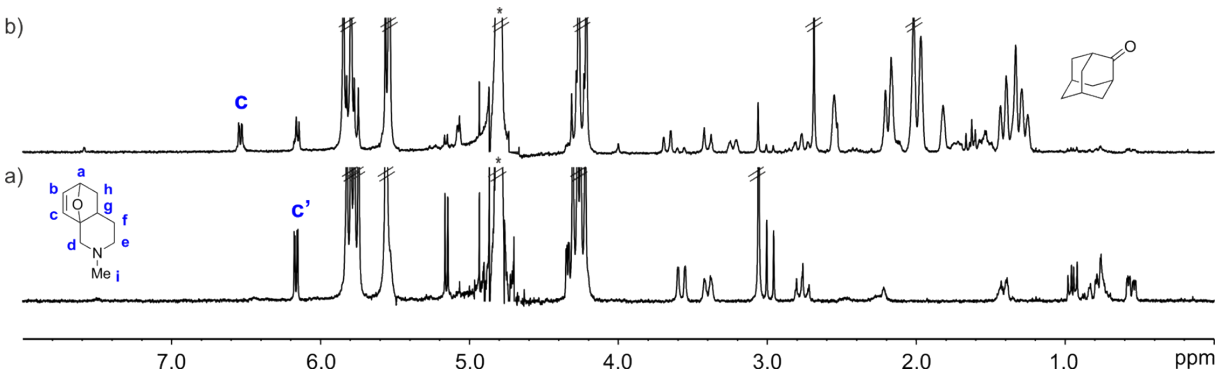

Figure S39. ^{1}H NMR spectra (300 MHz, D_2O, 298 K) of: a) **P-2⊂CB[7]** (1:1, 0.005 M), and b) addition of **ADA** to a). Primed labels correspond to proton signals of bound guest in **P-2⊂CB[7]**. *Residual solvent peak.

VI.3 Control Experiment

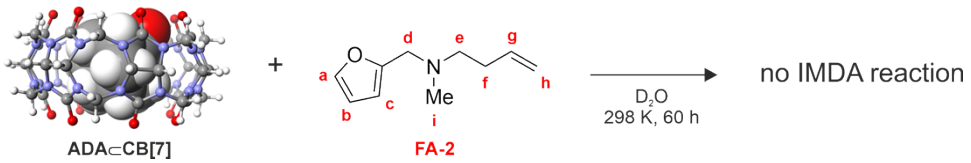

Scheme S4. Control experiment: addition of 1.0 equiv. of **FA-2** into a solution containing the preformed **ADA⊂CB[7]** complex.

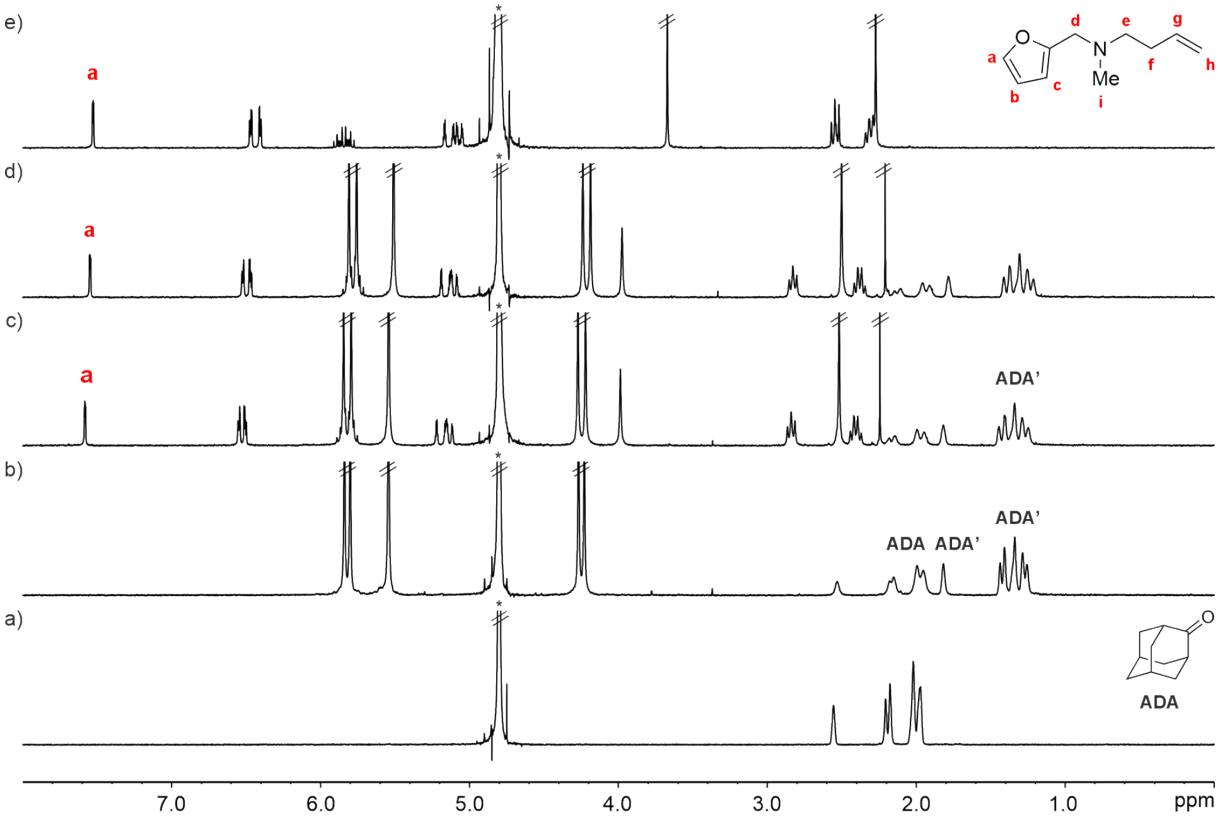

Figure S40. ^{1}H NMR spectra (300 MHz, D_2O, 298 K) of: a) **ADA**, b) **ADA⊂CB[7]** (2:1, 0.005 M), c) addition of **FA-2** (0.005 M) to **ADA⊂CB[7]** (2:1, 0.005 M), d) acquired after 60 h of spectrum c, and e) **FA-2** (0.005 M). **FA-2** in red and **ADA** in black. Primed labels correspond to proton signals of bound molecules. *Residual solvent peak.

VI.4 Kinetics upon Catalytic Amount of CB[7]

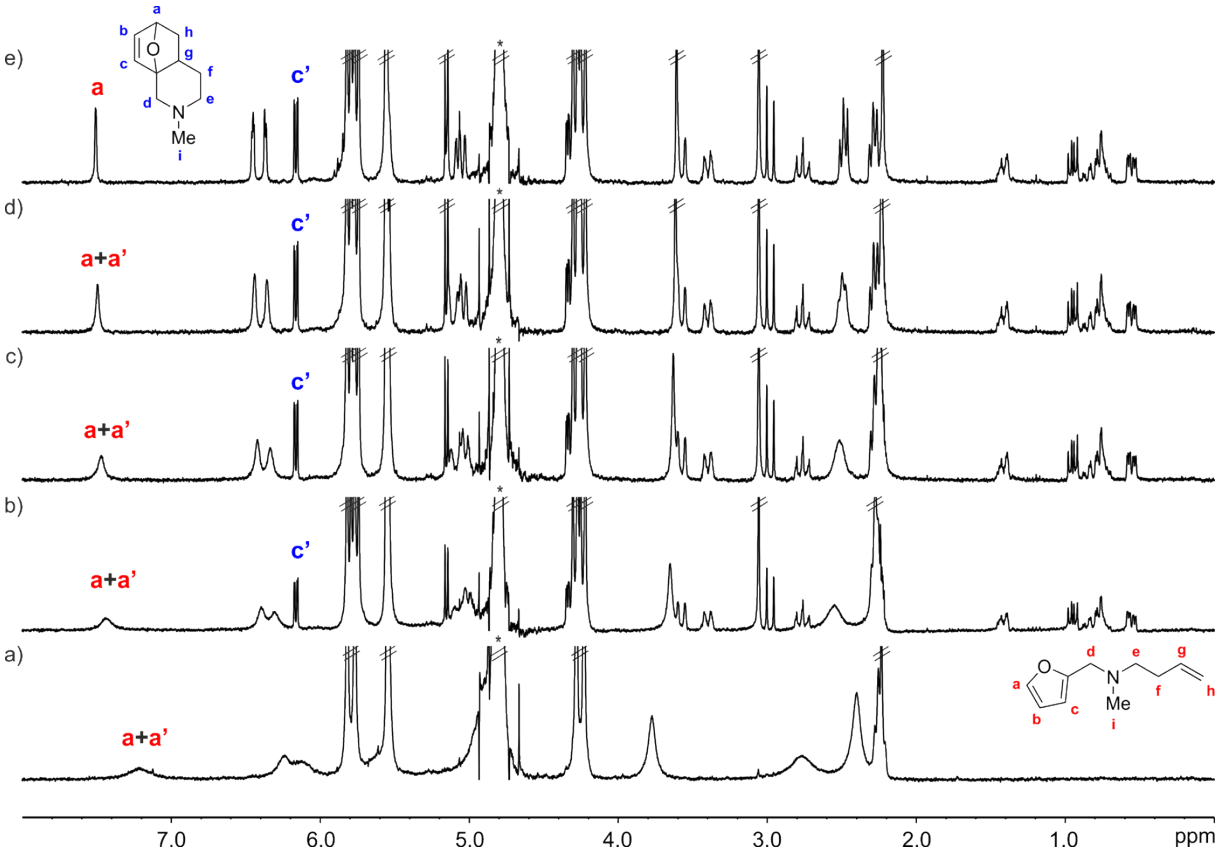

Figure S41. ^{1}H NMR spectra (300 MHz, D_2O, 298 K) of: a) **FA-2⊂CB[7]** (1:0.5, 0.01 M); and evolution of the IMDA reaction of **FA-2** (0.01 M) in the presence of **CB[7]** (0.5 equiv.) after: b) 8 h, c) 12 h, d) 20 h, and e) 48 h. **FA-2** in red and **P-2** in blue. Primed labels correspond to proton signals of bound molecules. *Residual solvent peak.

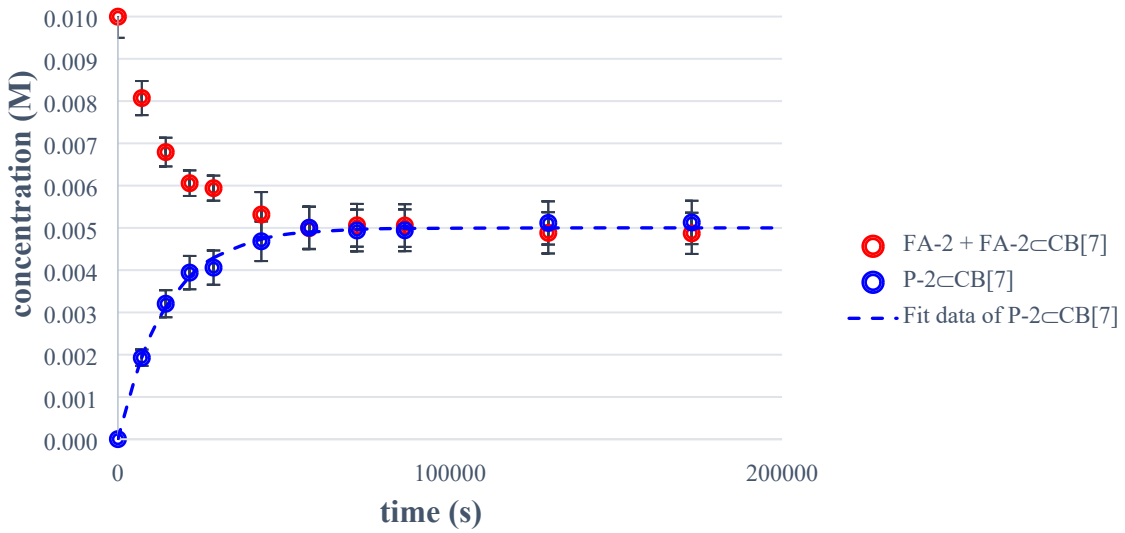

Figure S42. Plot of the concentrations (M) *vs.* time (s) for the IMDA reaction of **FA-2** (0.01 M) with **CB[7]** (0.5 equiv.) in D_2O at 298 K. Dashed line represents the fit of the experimental data to the theoretical kinetic simplified model 2 (Section IV). Error bars are standard deviations.

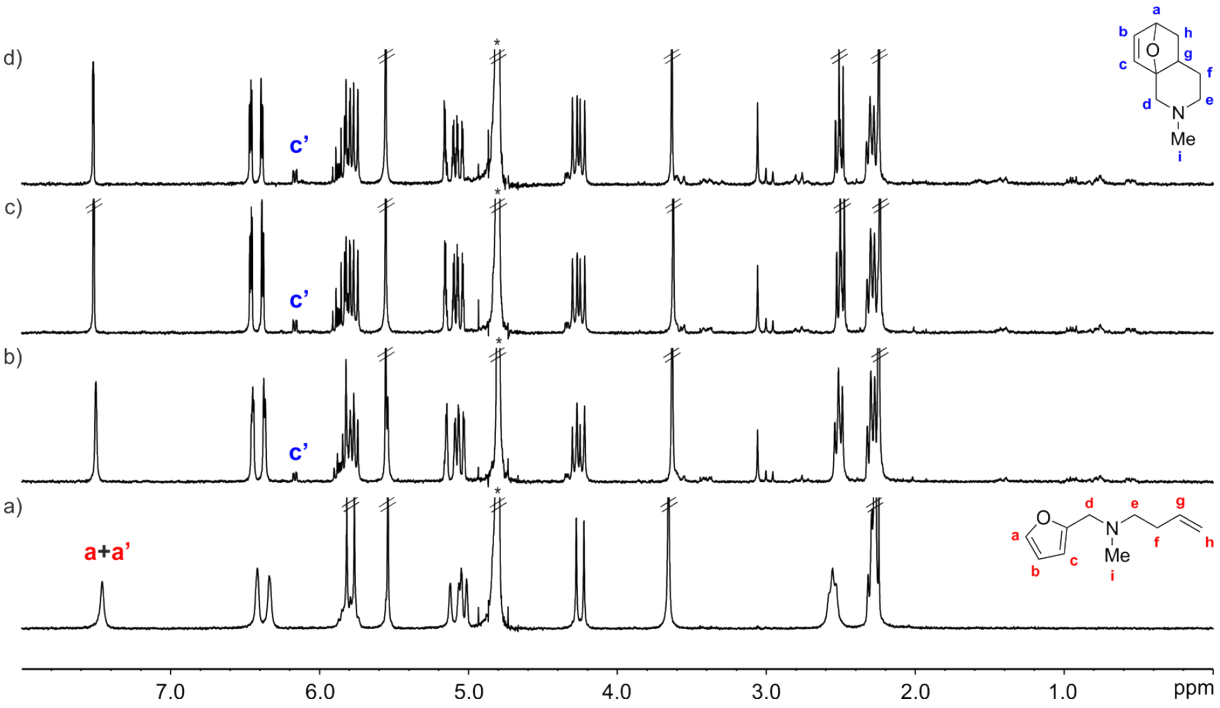

Figure S43. ^{1}H NMR spectra (300 MHz, D_2O, 298 K) of: a) **FA-2⊂CB[7]** (1:0.1, 0.01 M); and evolution of the IMDA reaction of **FA-2** (0.01 M) in the presence of **CB[7]** (0.1 equiv.) after: b) 8 h, c) 48 h, and d) 180 h. **FA-2** in red and **P-2** in blue. Primed labels correspond to proton signals of bound molecules. *Residual solvent peak.

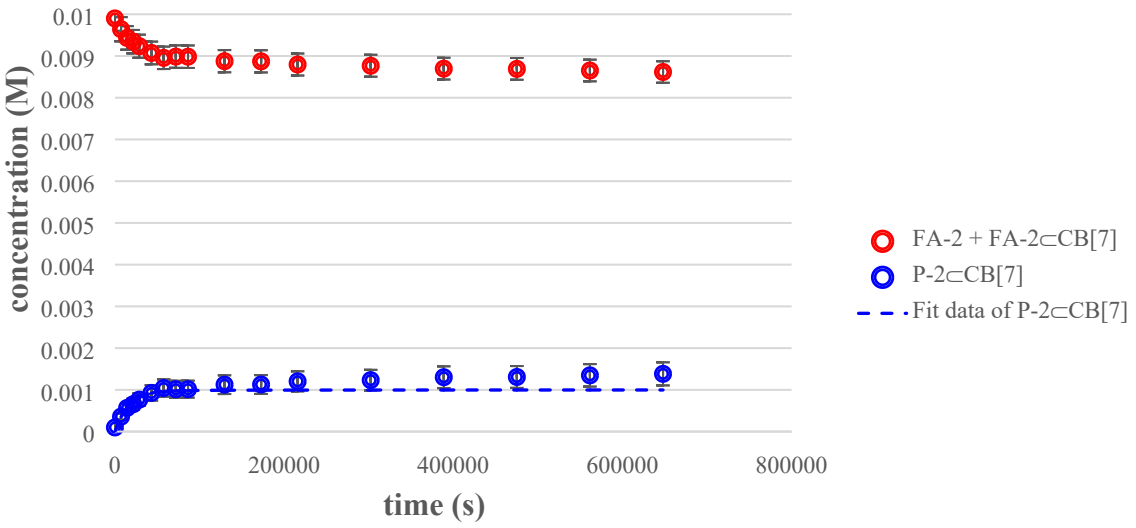

Figure S44. Plot of the concentrations (M) *vs.* time (s) for the IMDA reaction of **FA-2** (0.01 M) with **CB[7]** (0.1 equiv.) in D_2O at 298 K. Dashed line represents the fit of the experimental data to the theoretical kinetic simplified model 2 (Section IV). Error bars are standard deviations.

Table S9. Rate constant value and exchange rates used for the fitting of the reaction profile represented in Figure S44 (**FA-2** (0.01 M) with **CB[7]** (0.1 equiv.) in D_2O at 298 K), and calculated value for $k_{included}$. Error value in $k_{included}$ is reported as standard deviation.

Reaction	Constant
FA-2 → P-2	k_{bulk} = 1.0 x 10^{-8} s^{-1} [a]
FA-2 + CB[7] → FA-2⊂CB[7]	k_{on} (**FA-2⊂CB[7]**) = 5.5 x 10^3 $M^{-1}{\cdot}s^{-1}$ [b]
FA-2⊂CB[7] → FA-2 + CB[7]	k_{off} (**FA-2⊂CB[7]**) = 1.0 s^{-1} [b]
FA-2⊂CB[7] → P-2⊂CB[7]	$k_{included}$ = (5.8 ± 0.6) x 10^{-5} s^{-1}

[a] Estimated rate constant of the IMDA reaction of **FA-2** in the bulk at 298 K. [b] Estimated from K_a = k_{on}/k_{off} = 5.5 x 10^3 M^{-1} and assuming k_{off} = 1.0 s^{-1}.

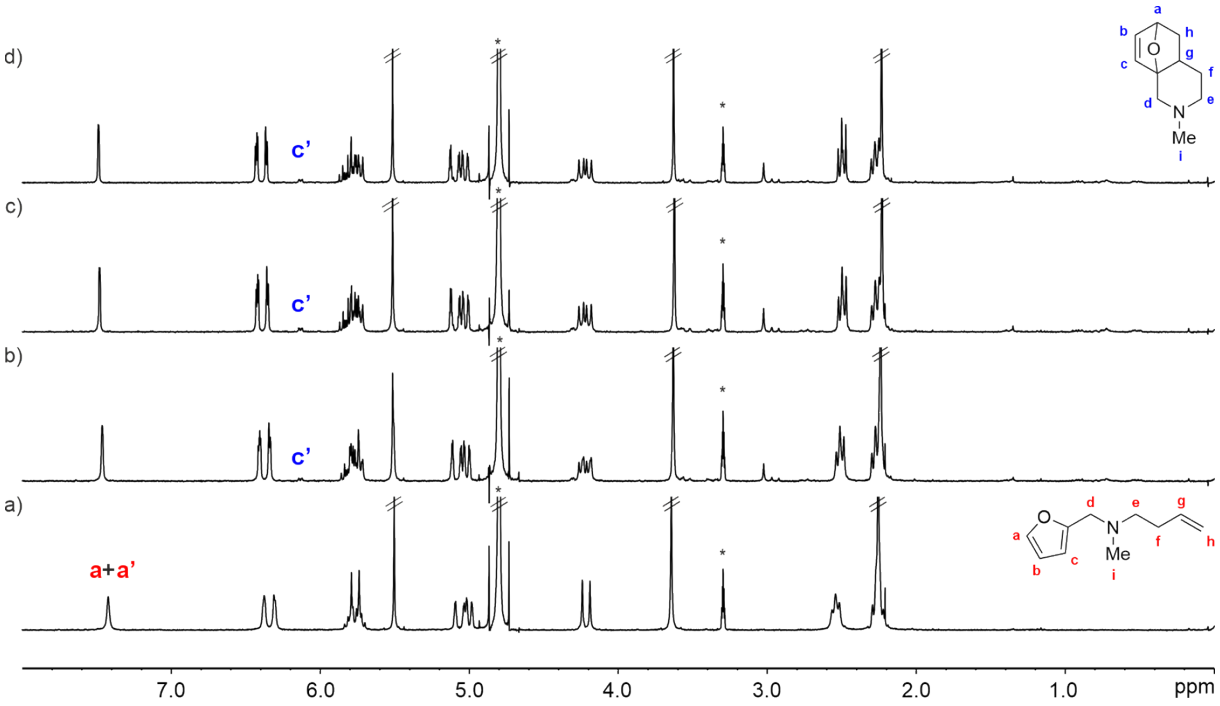

Figure S45. ^1H NMR spectra (300 MHz, D_2O:CD_3OD 9:1, 298 K) of: a) **FA-2⊂CB[7]** (1:0.1, 0.01 M); and evolution of the IMDA reaction of **FA-2** (0.01 M) in the presence of **CB[7]** (0.1 equiv.) after: b) 8 h, c) 20 h, and d) 108 h. *Residual solvent peaks.

VI.5 Determination of Activation Parameters under Standard Reaction Conditions

The IMDA cycloaddition reactions were run at least in duplicate at 298 K, 318 K, and 328 K. The rate constants were determined for each temperature in the presence of the container (the kinetic profiles for the reactions performed with **CB[7]** are shown henceforward). In the absence of the container, the rate constants were derived from the method of initial rates, except at 298 K since the product was never detected.

Table S10. Rate constant values determined by fitting the experimental data to the theoretical kinetic model with the Time Course and Parameter Estimation modules of COPASI Software Version 4.25 ($k_{included}$) or derived from the method of initial rates (k_{bulk}). Error values in $k_{included}$ are reported as standard deviations, while error values in initial rates are propagated to k_{bulk}.

System	T (K)	$k_{included}$ (s^{-1})	System	T (K)	k_{bulk} (s^{-1})
FA-2⊂CB[7]	298	$(1.2 \pm 0.1) \times 10^{-4}$	**FA-2**	298	$< 10^{-8}$
FA-2⊂CB[7]	318	$(5.6 \pm 0.1) \times 10^{-4}$	**FA-2**	318	$(4.1 \pm 0.1) \times 10^{-8}$
FA-2⊂CB[7]	328	$(1.1 \pm 0.1) \times 10^{-3}$	**FA-2**	328	$(7.8 \pm 0.1) \times 10^{-8}$

Similar to Figure S32, plotting ln(k/T) vs. 1/T (Eyring plot) resulted in a straight line (Figure S46), and fitting data to eq. 1 provided the activation enthalpy and entropy ($\Delta H^{\neq}$, $\Delta S^{\neq}$).

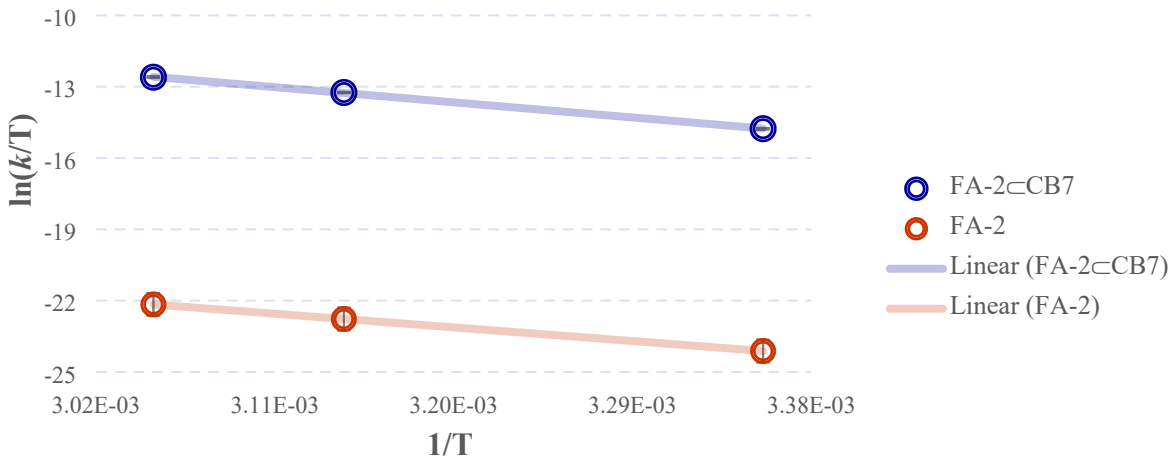

Figure S46. Eyring plots for **FA-2⊂CB[7]** (1:1, 0.005 M), and **FA-2** (0.005 M) in D_2O. Error bars are standard deviations.

The activation parameters of the IMDA reactions of **FA-2⊂CB[7]** (1:1, 0.005 M), and **FA-2** (0.005 M) in D_2O are summarized in the following table:

Table S11. Activation parameters of the IMDA reactions of **FA-2⊂CB[7]** (1:1, 0.005 M), and **FA-2** (0.005 M) in D_2O. Error values in $\Delta H^{\neq}$ and $\Delta S^{\neq}$ are reported as standard deviations and propagated to $\Delta G^{\neq}$.

System	$\Delta H^{\neq}$ [kcal·mol^{-1}]	$\Delta S^{\neq}$ [cal·mol^{-1}·K^{-1}]	$T\Delta S^{\neq}$ [kcal·mol^{-1}] [a]	$\Delta G^{\neq}$ [kcal·mol^{-1}] [a]
FA-2⊂CB[7]	14.1 ± 0.8	-29.3 ± 2.7	-8.7 ± 0.8	22.8 ± 1.1
FA-2	12.8 ± 0.4	-52.6 ± 1.4	-15.7 ± 0.4	28.4 ± 0.6

[a] 298 K.

Kinetic profiles for the reactions performed with **FA-2⊂CB[7]** (1:1, 0.005 M) at 318 K and 328 K:

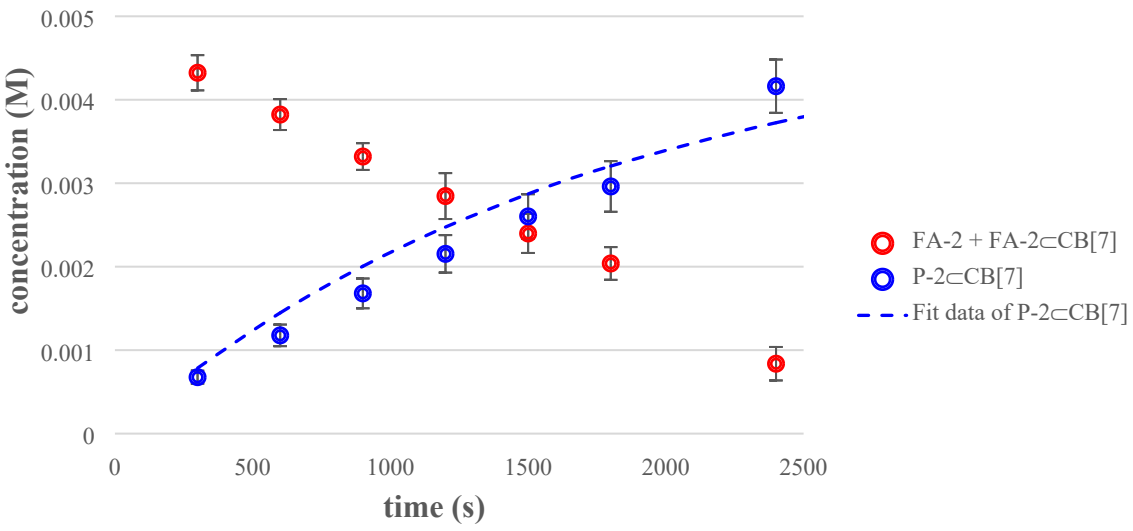

Figure S47. Plot of the concentrations (M) *vs.* time (s) for the IMDA reaction of **FA-2** (0.005 M) with **CB[7]** (1.0 equiv.) in D_2O at 318 K. Dashed line represents the fit of the experimental data to the theoretical kinetic simplified model 2 (Section IV). Error bars are standard deviations.

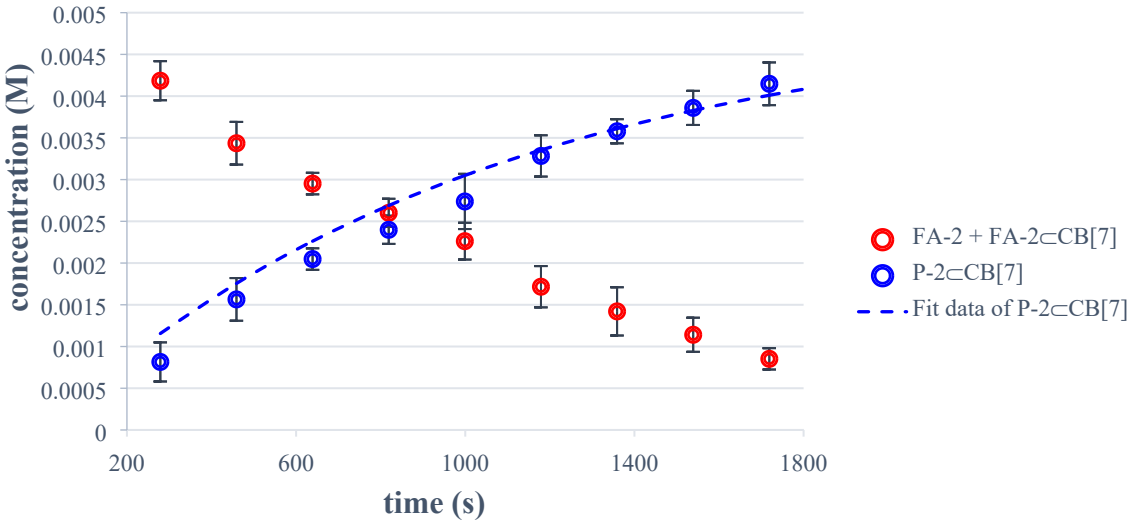

Figure S48. Plot of the concentrations (M) *vs.* time (s) for the IMDA reaction of **FA-2** (0.005 M) with **CB[7]** (1.0 equiv.) in D_2O at 328 K. Dashed line represents the fit of the experimental data to the theoretical kinetic simplified model 2 (Section IV). Error bars are standard deviations.

VII. Kinetic Studies of FA-1 with CB[8]

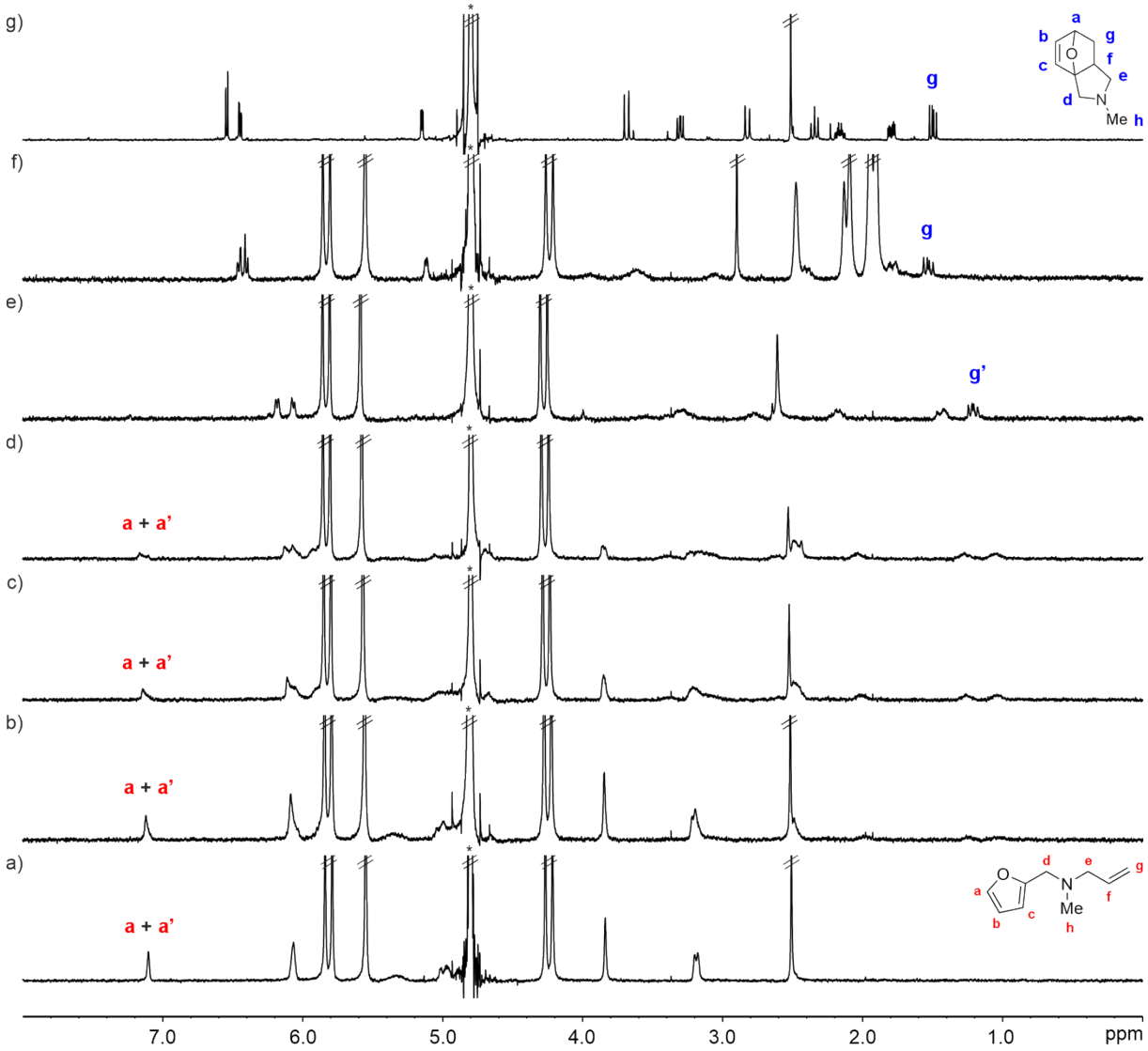

Figure S49. ^{1}H NMR spectra (300 MHz, D_2O, 298 K) of: a) **FA-1⊂CB[8]** (1:1, 0.0025 M); and evolution of the IMDA reaction of **FA-1** (0.0025 M) included in **CB[8]** (1.0 equiv.) after: b) 12 h, c) 36 h, d) 60 h, and e) 228 h. f) Addition of **ADA** to spectrum e) for the competitive displacement of **P-1**. g) ^{1}H NMR spectrum of **P-1**. **FA-1** in red and **P-1** in blue. Primed labels correspond to proton signals of bound molecules. *Residual solvent peak.

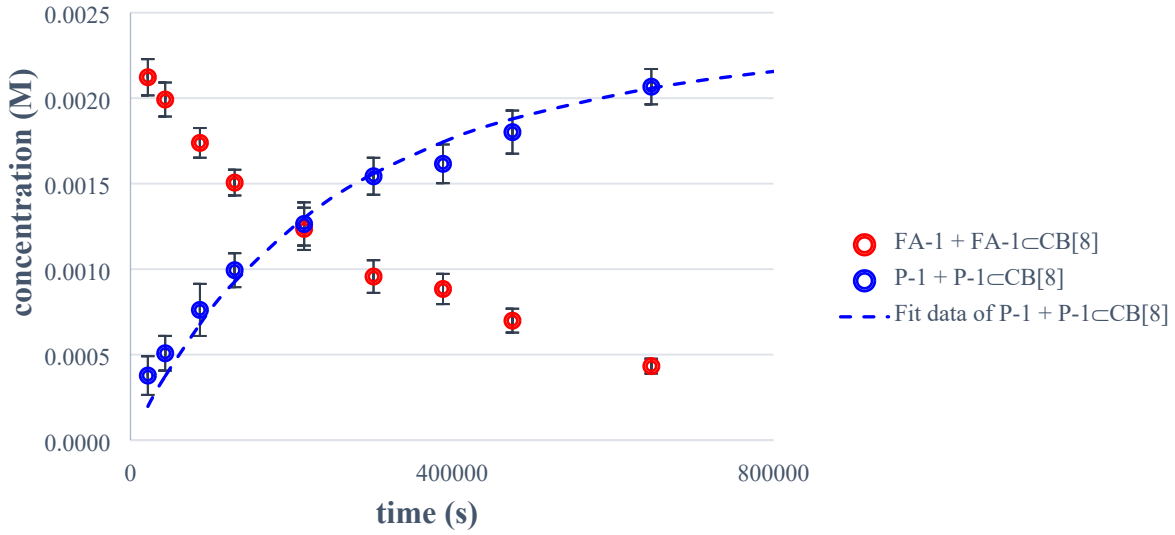

Figure S50. Plot of the concentrations (M) *vs.* time (s) for the IMDA reaction of **FA-1** (0.0025 M) with **CB[8]** (1.0 equiv.) in D_2O at 298 K. Dashed lines represent the fit of the experimental data to the theoretical simplified kinetic model 2 (Section IV). Error bars are standard deviations.

Table S12. Exchange rates of **FA-1⊂CB[8]** used for the fitting of the reaction profile represented in Figure S50 (**FA-1** (0.0025 M) with **CB[8]** (1.0 equiv.) in D_2O at 298 K), and calculated rate constant value for the IMDA reaction ($k_{included}$). Error value in $k_{included}$ is reported as standard deviation.

Reaction	Constant
FA-1 → P-1	k_{bulk} = 1.1 x 10^{-7} s^{-1} [a]
FA-1 + CB[8] → FA-1⊂CB[8]	k_{on} (**FA-1⊂CB[8]**) = 1.0 x 10^{3} $M^{-1}{\cdot}s^{-1}$ [b]
FA-1⊂CB[8] → FA-1 + CB[8]	k_{off} (**FA-1⊂CB[8]**) = 1.0 s^{-1} [b]
FA-1⊂CB[8] → P-1⊂CB[8]	$k_{included}$ = (4.6 ± 0.1) x 10^{-6} s^{-1}

[a] Rate constant of the IMDA reaction of **FA-1** in the bulk at 298 K. [b] Estimated from a K_a value (**FA-1⊂CB[8]**) = k_{on}/k_{off} of the order of 10^3 M^{-1} and assuming k_{off} = 1.0 s^{-1}.

VIII. Kinetic Studies of FA-2 with CB[8]

FA-2 did not result in any observable conversion into **P-2** in the presence of **CB[8]** after 2 weeks, neither at 25 °C nor at 40 °C.

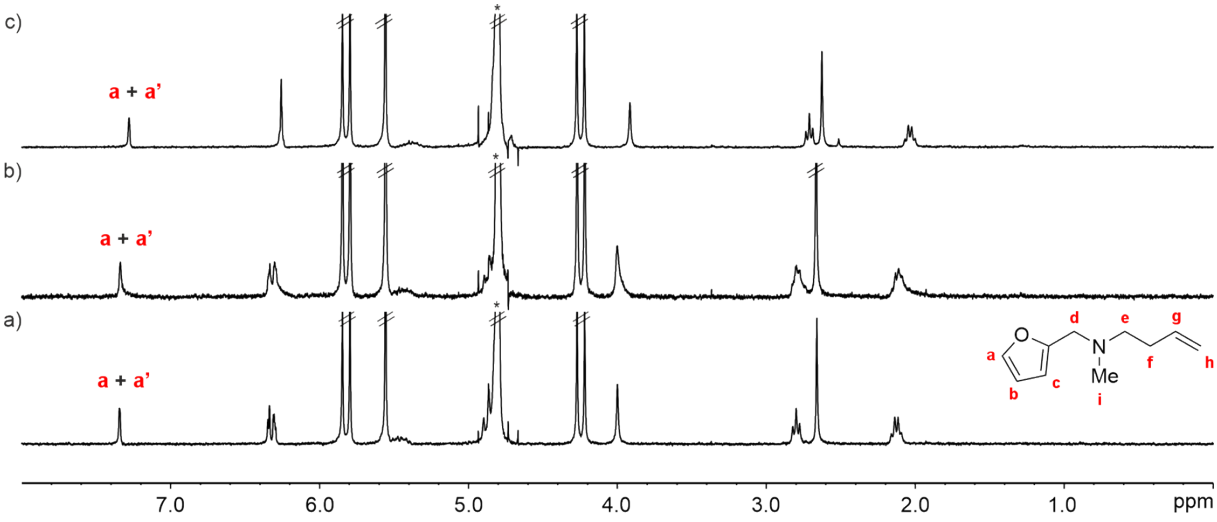

Figure S51. ^{1}H NMR spectra (300 MHz, D_2O, 298 K) of: a) **FA-2⊂CB[8]** (1:1, 0.0025 M); and evolution of **FA-2** (0.0025 M) included in **CB[8]** (1.0 equiv.) after: b) 2 weeks at 298 K, and c) 2 weeks at 313 K. Primed labels correspond to proton signals of bound molecules. *Residual solvent peak.

IX. Kinetic Data and CB[*n*]-promoted acceleration ($k_{included}/k_{bulk}$) of the IMDA cycloaddition reactions of FA-1 and FA-2

A summary of all determined rate constants is presented below, together with the reactions half-life, $t_{1/2}$, in the bulk and included in the **CB[*n*]s**, as well as the calculated acceleration factors.

Table S13. Kinetic data and CB[*n*]-promoted acceleration ($k_{included}/k_{bulk}$) of the IMDA cycloaddition reactions of **FA-1** and **FA-2** at different temperatures.

Guest [a]	CB[*n*] [b]	T (K)	$k_{included}$ (s^{-1}) [c]	$t_{1/2\text{-included}}$ (h) [d]	k_{bulk} (s^{-1}) [c]	$t_{1/2\text{-bulk}}$ (h) [d]	Acceleration ($k_{included}/k_{bulk}$)
FA-1	CB[7]	298	$(6.7 \pm 0.3) \times 10^{-5}$	2.87	$(1.1 \pm 0.1) \times 10^{-7}$	1693	590
FA-1	CB[7]	308	$(3.5 \pm 0.1) \times 10^{-4}$	0.55	$(5.9 \pm 0.2) \times 10^{-7}$	327	593
FA-1	CB[7]	318	$(1.1 \pm 0.1) \times 10^{-3}$	0.17	$(1.1 \pm 0.1) \times 10^{-6}$	173	1010
FA-1	CB[7]	328	$(2.9 \pm 0.1) \times 10^{-3}$	0.07	$(1.8 \pm 0.1) \times 10^{-6}$	110	1673
FA-2	CB[7]	298	$(1.2 \pm 0.1) \times 10^{-4}$	1.67	$< 10^{-8}$ [e]	> 19250	> 11499
FA-2	CB[7]	318	$(5.6 \pm 0.1) \times 10^{-4}$	0.34	$(4.1 \pm 0.1) \times 10^{-8}$ [f]	4695	13720
FA-2	CB[7]	328	$(1.1 \pm 0.1) \times 10^{-3}$	0.17	$(7.8 \pm 0.1) \times 10^{-8}$ [f]	2468	14149
FA-1 [g]	CB[8]	298	$(4.6 \pm 0.1) \times 10^{-6}$	40.6	$(1.1 \pm 0.1) \times 10^{-7}$	1693	41

[a] 0.005 M. [b] 1.0 equiv. [c] Rate constant values determined by fitting the experimental data to the theoretical kinetic model with the Time Course and Parameter Estimation modules of COPASI Software Version 4.25. Error values are reported as standard deviations. [d] Time required for the reactant concentration to decrease to one-half its initial value; for a first-order reaction, the half-life is determined: $t_{1/2} = 0.693/k$. [e] Estimated value. [f] Values derived from the method of initial rates. [g] 0.0025 M.

X. Binding and Kinetic Studies of FA-1 with Cyclodextrins

We decided to explore the binding of **FA-1** with α-, β- and γ-CDs, as well as its reactivity in the presence of the CD series. Using ^{1}H NMR titration experiments, we observed that **FA-1** was weakly bind by the cyclodextrins (α-, β- and γ-CDs). In all cases, we estimated that the binding constants K_a were lower than 10 M^{-1} from the fit of the titration data to a 1:1 binding model. After monitoring the solutions of **FA-1** with the CDs for 60 h using ^{1}H NMR spectroscopy, we did not observe any evidence of the formation of **P-1**.

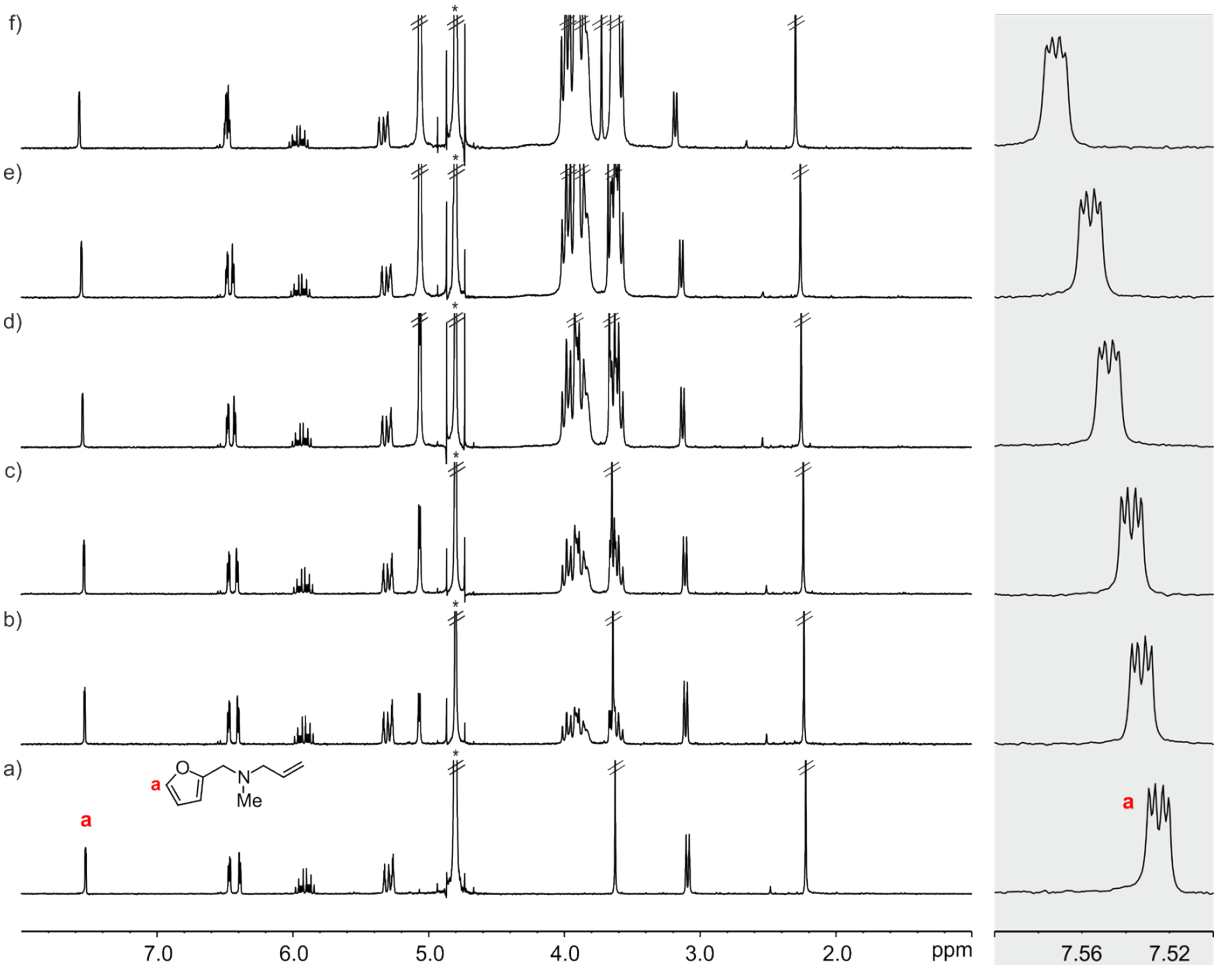

Figure S52. ^{1}H NMR spectra (300 MHz, D_2O, 298 K) of the titration experiment of **FA-1** (5.0 mM) with ***α*-CD**: a) 0 equiv., b) 0.25 equiv., c) 0.5 equiv., d) 1.0 equiv., e) 1.5 equiv., f) 2.0 equiv. Signals between 7.6 and 7.5 ppm are expanded in the gray box (right). Binding constant value (K_a) was derived from the fitting of the chemical shift changes of the titration data to a 1:1 theoretical binding model using HypNMR2008 software. K_a (**FA-1** ⊂ ***α*-CD**) < 10 M^{-1}. *Residual solvent peak.

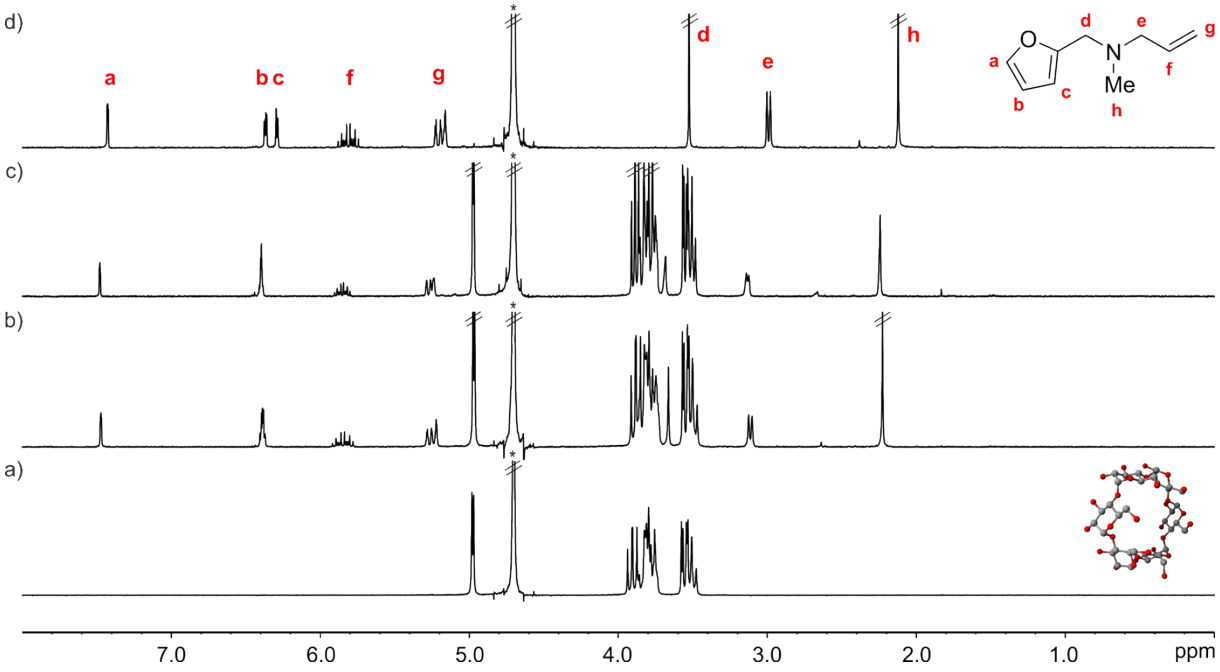

Figure S53. ^{1}H NMR spectra (300 MHz, D_2O, 298 K) of ***α*-CD** (5.0 mM) with **FA-1**: a) 0 equiv., b) 2.0 equiv., c) 2.0 equiv. after 60 h. d) ^{1}H NMR spectrum of **FA-1**. *Residual solvent peak.

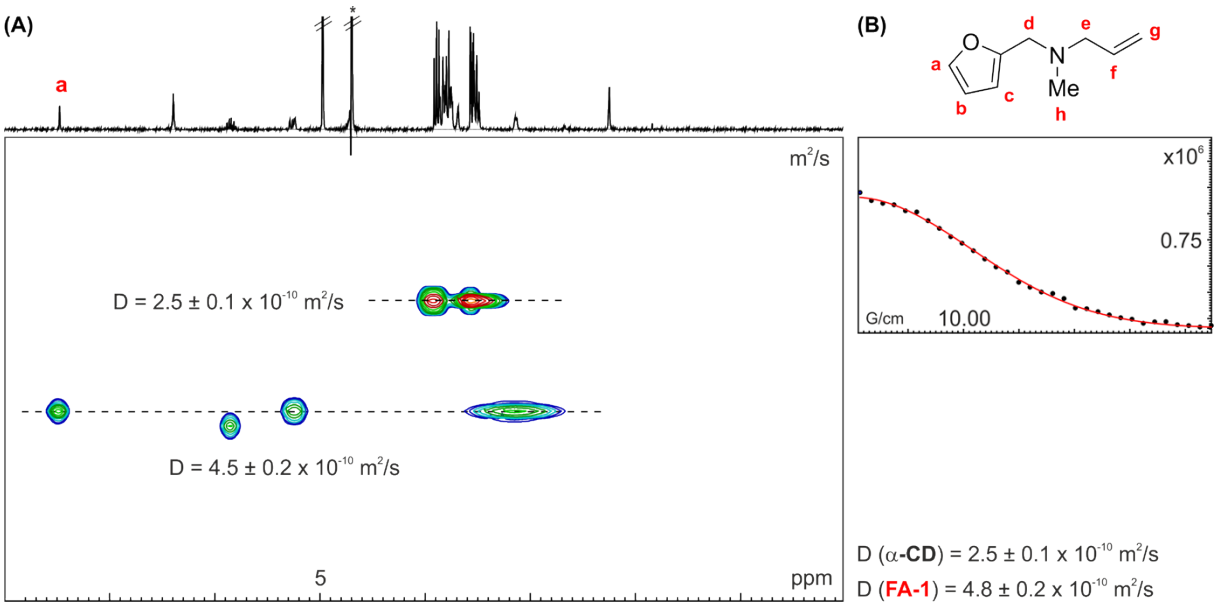

Figure S54. (A) ^{1}H pseudo 2D plot of DOSY (400 MHz, D_2O, 298 K, D20 = 0.15 s; P30 = 1.5 ms) of ***α*-CD** (10 mM) with **FA-1** (0.5 equiv.). (B) Fit of the decay of signal **a** to a mono-exponential function using Dynamics Center from Bruker. Errors are indicated as standard deviations. Diffusion coefficients for unbound substrate **FA-1** and unbound host ***α*-CD** are provided for the ease of comparison (right bottom). *Residual solvent peak.

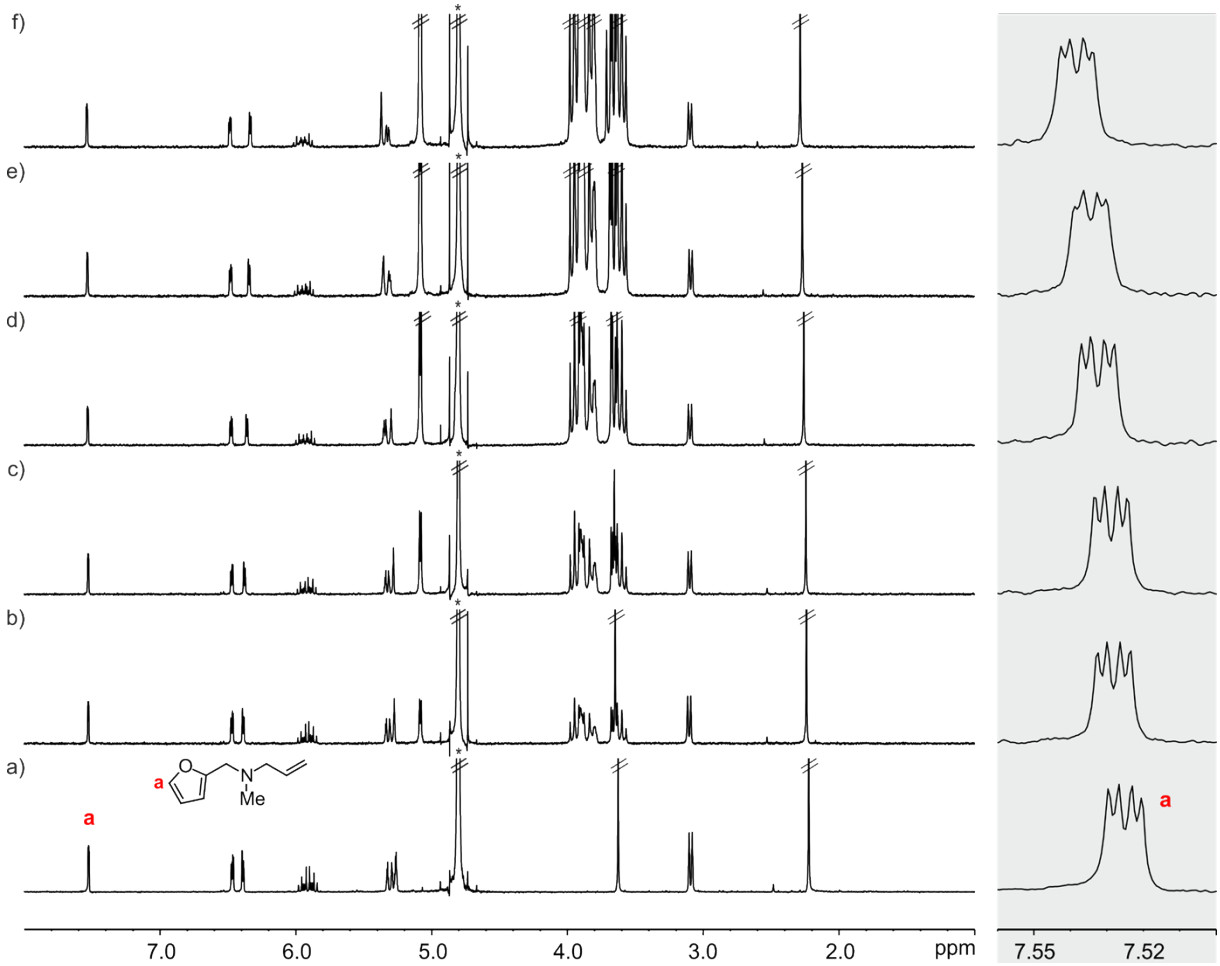

Figure S55. ^{1}H NMR spectra (300 MHz, D_2O, 298 K) of the titration experiment of **FA-1** (2.5 mM) with **β-CD**: a) 0 equiv., b) 0.25 equiv., c) 0.5 equiv., d) 1.0 equiv., e) 1.5 equiv., f) 2.0 equiv. Signals between 7.56 and 7.50 ppm are expanded in the gray box (right). Binding constant value (K_a) was derived from the fitting of the chemical shift changes of the titration data to a 1:1 theoretical binding model using HypNMR2008 software. K_a (**FA-1** ⊂ **β-CD**) < 10 M^{-1}. *Residual solvent peak.

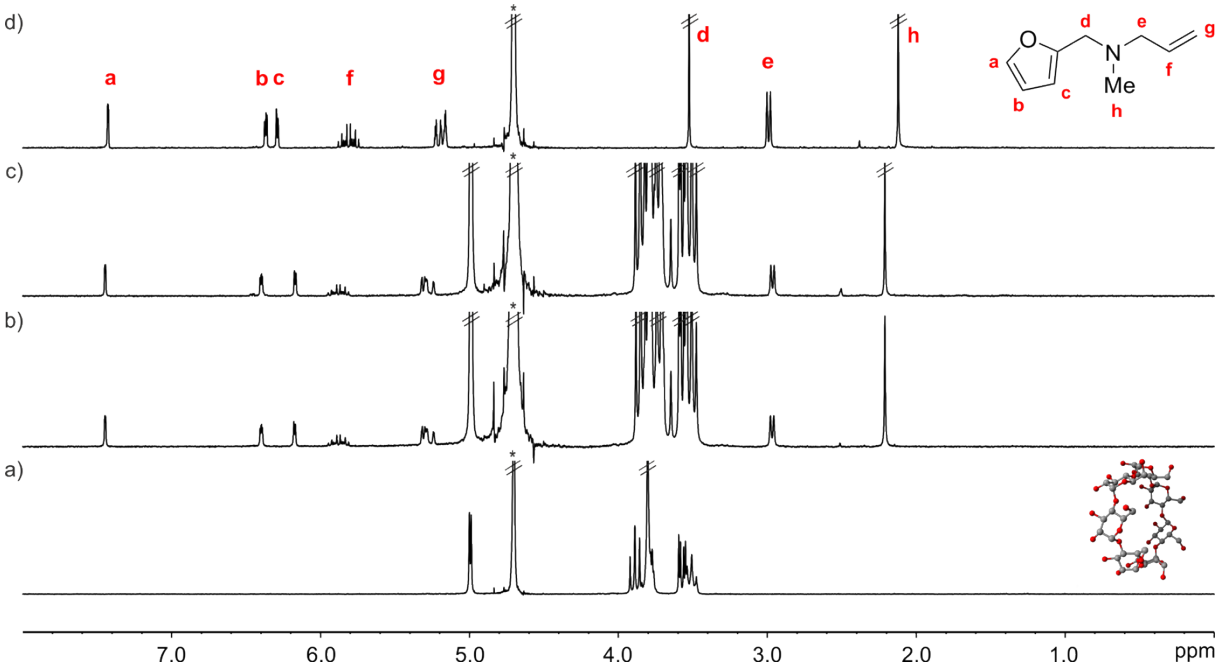

Figure S56. ^{1}H NMR spectra (300 MHz, D_2O, 298 K) of **β-CD** (5.0 mM) with **FA-1**: a) 0 equiv., b) 2.0 equiv., c) 2.0 equiv. after 60 h. d) ^{1}H NMR spectrum of **FA-1**. *Residual solvent peak.

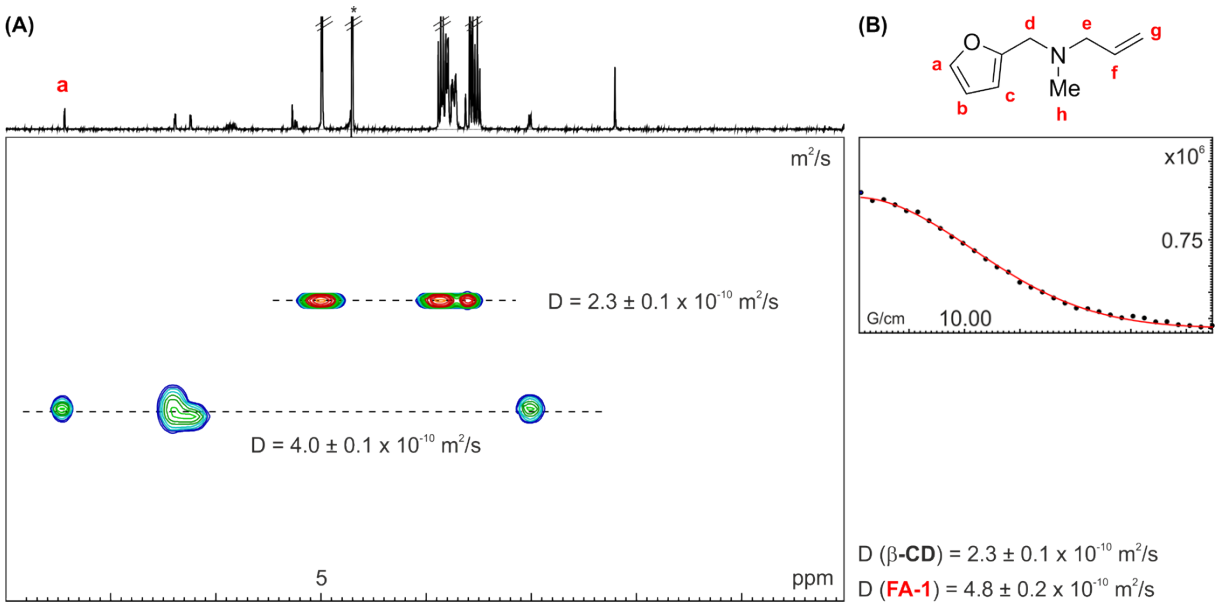

Figure S57. (A) ^{1}H pseudo 2D plot of DOSY (400 MHz, D_2O, 298 K, D20 = 0.15 s; P30 = 1.5 ms) of **β-CD** (5.0 mM) with **FA-1** (0.5 equiv.). (B) Fit of the decay of signal **a** to a mono-exponential function using Dynamics Center from Bruker. Errors are indicated as standard deviations. Diffusion coefficients for unbound substrate **FA-1** and unbound host **β-CD** are provided for the ease of comparison (right bottom). *Residual solvent peak.

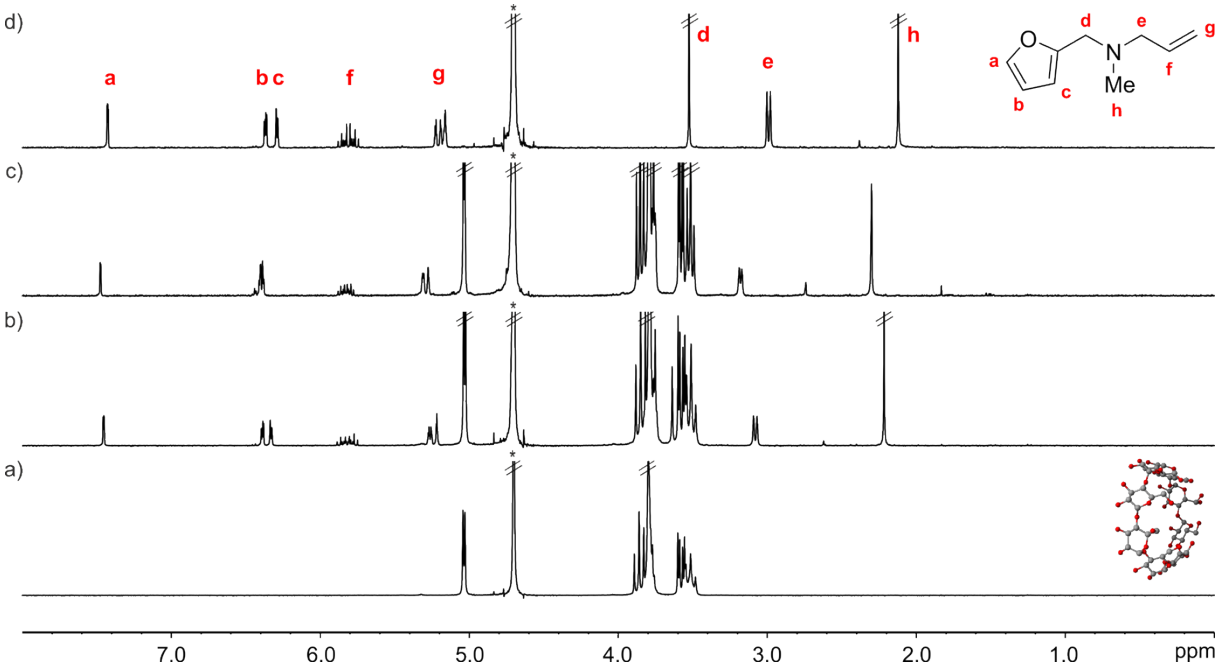

Figure S58. ^{1}H NMR spectra (300 MHz, D_2O, 298 K) of **γ-CD** (5.0 mM) with **FA-1**: a) 0 equiv., b) 1.0 equiv., c) 1.0 equiv. after 60 h. d) ^{1}H NMR spectrum of **FA-1**. *Residual solvent peak.

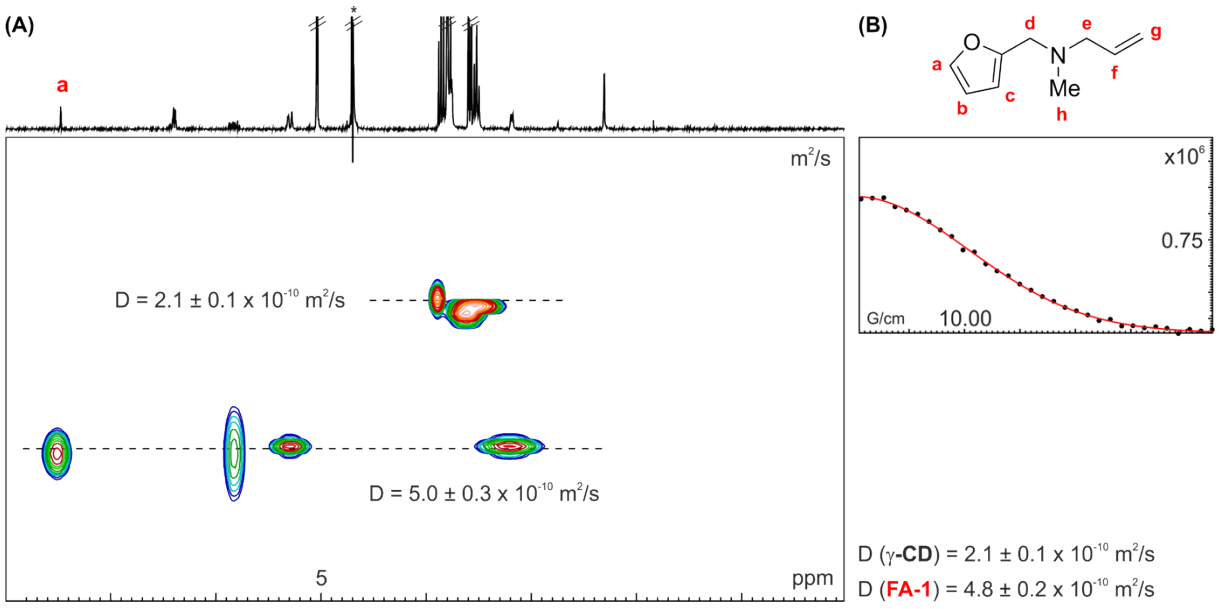

Figure S59. (A) ^{1}H pseudo 2D plot of DOSY (400 MHz, D_2O, 298 K, D20 = 0.15 s; P30 = 1.5 ms) of **γ-CD** (5.0 mM) with **FA-1** (1.0 equiv.). (B) Fit of the decay of signal **a** to a mono-exponential function using Dynamics Center from Bruker. Errors are indicated as standard deviations. Diffusion coefficients for unbound substrate **FA-1** and unbound host **γ-CD** are provided for the ease of comparison (right bottom). *Residual solvent peak.

XI. Energy-Minimized Structures of the Inclusion Complexes with CB[*n*]s

Molecular modeling was performed using the semiempirical method PM6 in Scigress Version FJ 2.6.

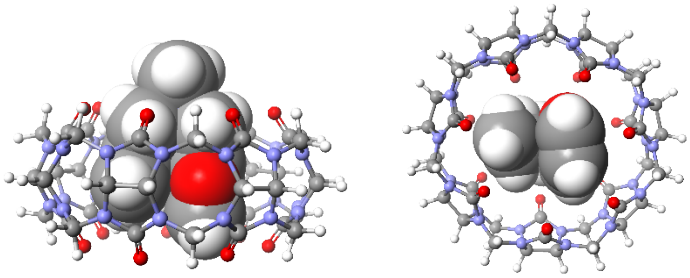

Figure S60. Energy-minimized structure (PM6) of the 1:1 inclusion complex of **FA-1** with **CB[7]**. The host is depicted in ball-and-cylinder representation and the bound guest is shown as CPK model.

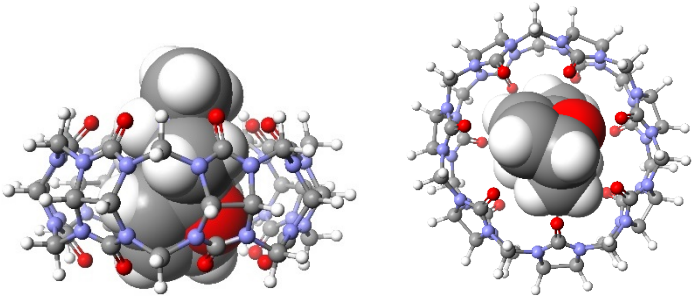

Figure S61. Energy-minimized structure (PM6) of the 1:1 inclusion complex of **P-1** with **CB[7]**. The host is depicted in ball-and-cylinder representation and the bound guest is shown as CPK model.

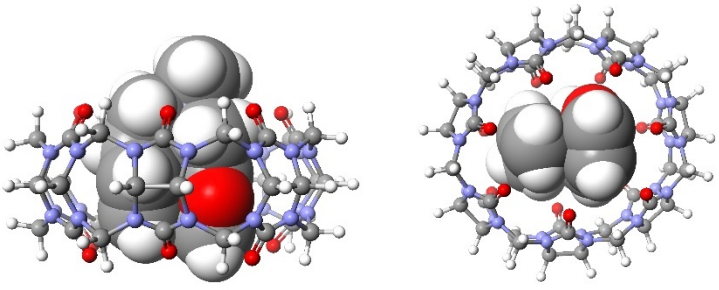

Figure S62. Energy-minimized structure (PM6) of the 1:1 inclusion complex of **FA-2** with **CB[7]**. The host is depicted in ball-and-cylinder representation and the bound guest is shown as CPK model.

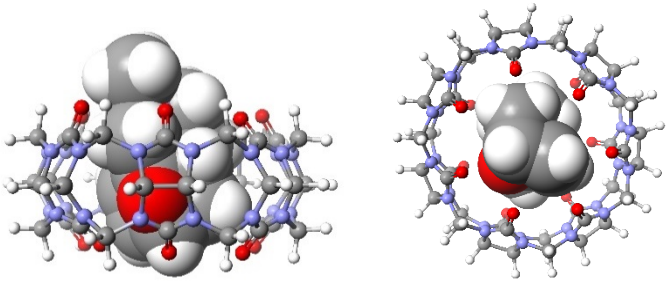

Figure S63. Energy-minimized structure (PM6) of the 1:1 inclusion complex of **P-2** with **CB[7]**. The host is depicted in ball-and-cylinder representation and the bound guest is shown as CPK model.

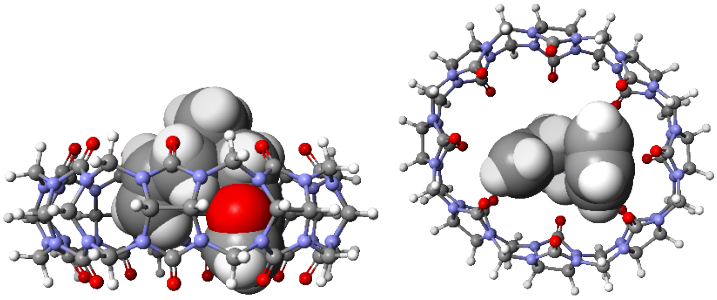

Figure S64. Energy-minimized structure (PM6) of the 1:1 inclusion complex of **FA-1** with **CB[8]**. The host is depicted in ball-and-cylinder representation and the bound guest is shown as CPK model.

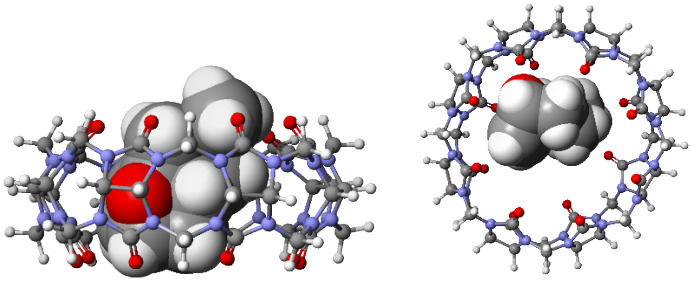

Figure S65. Energy-minimized structure (PM6) of the 1:1 inclusion complex of **P-1** with **CB[8]**. The host is depicted in ball-and-cylinder representation and the bound guest is shown as CPK model.

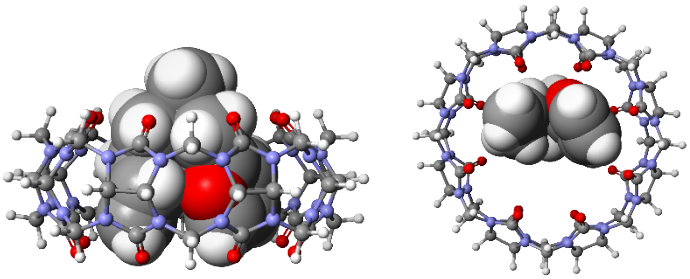

Figure S66. Energy-minimized structure (PM6) of the 1:1 inclusion complex of **FA-2** with **CB[8]**. The host is depicted in ball-and-cylinder representation and the bound guest is shown as CPK model.

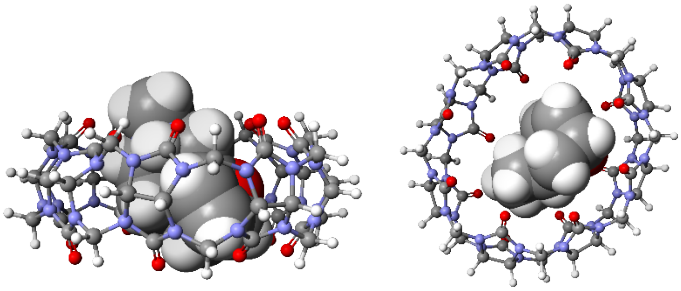

Figure S67. Energy-minimized structure (PM6) of the 1:1 inclusion complex of **P-2** with **CB[8]**. The host is depicted in ball-and-cylinder representation and the bound guest is shown as CPK model.